Vol. 2 February 2016

AOFPR

Asian and Oceanic Forum for Paediatric Radiology











CONTENTS

From the Editorial board

Invited Articles

Case Reports

Asian and Oceanic Forum for Paediatric Radiology

Bernard F. Laya MD, DO, FPCR

Professor of Radiology and Associate Dean, St. Luke's College of Medicine — WHQM
Head, Institute of Radiology, St. Luke's Medical Center — Global City, Philippines

Pediatric Radiology: Providing Optimum Healthcare Delivery in Children Through Medical Imaging

Soon after Wilhelm Conrad Röntgen discovered x-rays on November 8, 1895, he sent details of his discovery to physicists throughout the world and it was warmly received. Others replicated his discovery and many of the earliest radiographic examinations were of infants and children. Earlier indications for x-ray were trauma, foreign body search, skeletal maturation and variations, but these indications have rapidly expanded to include inherited disorders, inflammatory processes and tumors. With the introduction of advanced imaging modalities and technique, medical imaging has become a vital component of healthcare delivery particularly in children.

It is without a doubt that pediatric radiology is one of the oldest subspecialty in radiology. It deals with diagnosis and sometimes treatment of illnesses in infants, children and young adults utilizing various medical imaging techniques. This field also includes advanced imaging of fetal abnormalities. "Children are not small adults", for diseases and its manifestations in children are generally different with that of adults. Some cancers are only found in children, such as Wilms' tumor and neuroblastoma, and there are other conditions seen only in newborn or premature infants. A child's body mechanics and response to injury or stress is also different from an adult, and children have an immature immune system making them a lot more prone to infections. In addition to acquired illnesses, a unique group of congenital malformations are also common in pediatric population. Not only is there a difference in the disease process, the approach to therapy and care of an ailing child is also different from that of an adult.

Having gone through specialized training, a pediatric radiologist is equipped with the general knowledge of childhood diseases as it relates to imaging. Pediatric radiology practitioners not only deal with their patients, but they also have to deal with the parents as well as the pediatricians and primary care providers. As an expert, the pediatric radiologist is not only responsible for interpreting the imaging findings, but also makes sure that the appropriate study is performed safely and for the right indication. Ultimately, the pediatric radiologist communicates with the pediatrician or any referring consultant about the disease, the choice of imaging study, treatment and even follow up.

There are now global initiatives to improve and standardize medical imaging in children, which include the Image Gently campaign of the American College of Radiology (ACR) and Society for Pediatric Radiology (SPR), as well as the EuroSafe Imaging campaign of the European Society of Radiology (ESR). There are also regional societies all over the world that promote education on imaging diagnosis but also highlight the best imaging practices for the benefit of children. The newly formed World Federation of Pediatric Imaging (WFPI) helps in bridging these various international organizations including those that belong to lower resource settings. There is much more to learn and accomplish and the pediatric imaging community is determined to do just that.

The Asian and Oceanic Society for Pediatric Radiology (AOSPR) was formed in June 2000 under the leadership of the founding president Prof. Mutsuhisa Fujioka. The main objective is to improve healthcare standards in the imaging of children in the Asia-Oceanic region through cooperative research, teaching and education. One of the organization's activities is the yearly AOSPR congress that is held in various his-

torical, scenic, and exotic cities of Asia and Oceania. These meetings are a venue for solid continuing education with exchange of ideas, at the same time fostering camaraderie and stronger bond among its now 322 members from Asia, Oceanea, and beyond. The AOSPR website is an ongoing dynamic project which serves as an avenue to educate and communicate, but the introduction of Asian and Oceanic forum for Pediatric Radiology (AOfPR) in 2015 is an important milestone that further enhances this objective.

Although the practice of pediatric radiology is standardized and deemed a necessity in the western world and progressive countries of Asia, such is not the case in developing Asian countries. In the Philippines, the practice of radiology is unique because other than breast imaging and interventional radiology, the subspecialty societies and fellowship training available are modality-based (ultrasound, CT, and MRI). This being the norm, it poses inherent limitation to the practice and advancement of organ system-based radiology and specialized fields of interest, including pediatric radiology. Despite the small number and the absence of national acceptance brought about by the local practice standards, pediatric radiology practitioners in the Philippines continue to thrive with the aim to raise the level of healthcare delivery through imaging in the country. Philippine pediatric radiologists maintain a respectable stature in the international scientific community as contributors to current knowledge through their lectures, publications and researches, raising awareness about the subspecialty.

In a field of medicine that is constantly changing, it is very important to keep abreast with the current literature in order to be of better service to both patients and referring clinicians. The introduction of AOfPR is helpful in this endeavor. Since its initial release last year, the forum has gained support and following due to its education-focused format tackling pertinent, current, and must know topics in various subspecialties of pediatric radiology. Its open access, online format makes it even more appealing because it is readily available to everyone for free.

I would like to thank the AOSPR leadership, the AOfPR Editorial Board and the Webmasters for this honor and opportunity to serve the radiology community as a Guest Editor. I would also like to thank all of the authors in this issue for their hard work and outstanding contributions. My gratitude goes to the brother and sister team of Niko Bryan C. Sumaya and Dr. Amerrel C. Sumaya for the cover design showcasing various images and sights in the Philippines. I would also like to acknowledge and thank my colleagues, fellows, and residents at St. Luke's Medical Center, Philippines for their unwavering trust and support. Not to forget, I would like to thank my family for their unconditional love, support, and understanding.

It is with great pride that I present to you the current issue of AOfPR. I am certain that these articles will be very helpful in your radiology practice and I hope you enjoy reading them.

The Role of Computed Tomography Imaging in Children with Complex Congenital Cardiovascular Disease

Vincent Tatco, MD, Derrick Chansiongpen, MD and Maria Kristine Mendoza, MD

Institute of Radiology, St. Luke's Medical Center, Philippines

Abstract

The field of cardiac computed tomography imaging (CT) is evolving rapidly with the availability of new multidetector scanner technology. In addition, the prevalence of palliated congenital heart diseases (CHD) has increased with marked improvements in patient survival. Multidetector CT plays an important role in the pre- and postoperative evaluation of CHD in children. Despite radiation exposure, CT is commonly used for evaluation of the complex congenital cardiac and vascular anomalies, giving information on both intra- and extracardiac anatomy. Imaging small children with CHD is challenging, and in this review article we will discuss the fundamentals and essentials for performing CT, including basic techniques and imaging protocols, strengths, limitations and applications of this modality in the pediatric population.

Introduction

Congenital heart disease (CHD) remains a major cardiac problem and a significant cause of morbidity and mortality in pediatric patients. Advances in cardiovascular surgery and interventions have resulted to marked improvements in patient survival. Cardiac computed tomography (CT) imaging plays an important role in the diagnosis, interventional management, and follow-up after palliative or corrective surgery of this disease. It is a useful, rapid, and noninvasive imaging technique that can bridge the gaps between echocardiography, cardiac catheterization, and cardiac magnetic resonance imaging (MRI). Current multidetector CT techniques can accurately evaluate extracardiac great vessels, lungs, and airways, as well as coronary arteries and intracardiac structures [1—6]. Fast scan speed and greater anatomic coverage, combined with flexible ECG-synchronized scans and low radiation dose, are critical for improving the image quality of cardiac CT and minimizing patient risk. This review article will discuss the fundamentals and essentials for performing pediatric cardiac CT as well as the strengths, limitations and applications of this modality in evaluating children with CHD.

Methods

Scanner requirements

A multidetector CT scanner is a prerequisite in performing cardiac CT. As performance of a cardiac CT may pose some technical difficulties in young children, the use of multidetector CT offers the advantage of fast image acquisition and volume data generation, reduction of the radiation dose and improvement of image quality by using noise reduction algorithms. With the development of fast gantry rotation speed and wider collimation coverage, the scan duration is reduced, temporal resolution is increased, and hence motion artifacts are decreased [5]. In our institution, a 256-slice multidetector CT scanner (Brilliance iCT, Philips Healthcare, Cleveland, Ohio, USA) with electrocardiogram-gating (ECG-gating) capability is used to obtain isotropic volume data from which high-quality two- and three-dimensional multiplanar reformatted images can be generated to accurately and systematically delineate the normal and pathologic morphologic features of the cardiovascular system in patients with CHD.

Patient preparation and sedation

Patient preparation in our institution includes determination of possible contraindications for contrast administration (e.g., deranged kidney function) and fasting of at least 3 hours prior to the procedure. Premedication may be given to decrease the frequency of contrast medium adverse reactions in patients with history of asthma or allergies, based upon the discretion of the attending physician or radiologist.

Sedation is usually not necessary in neonates, calm babies, and cooperative children older than seven years of age [3—7]. For children who are agitated, uncooperative or unable to follow breath-hold instructions, referral to an anesthesiologist or pediatric cardiologist for sedation is done. Sedation prior to scanning prevents agitation during contrast delivery to children, avoiding the need for repeated examinations that increase radiation burden. Pharmacological heart rate manipulation using beta blockade is sometimes necessary in ECG-gated studies but is not used routinely. In our institution, the anesthesiologist or pediatric cardiologist is responsible for sedation and monitoring the patients. Vital signs and blood oxygen saturation must always be monitored. Medical personnel skilled in the management of cardiac emergencies must always accompany the patient.

Contrast medium injection and venous access

A volume of 2 ml/kg bodyweight of non-ionic iodinated contrast agent (300 mI/ml or more) is administered through a large bore IV cannula via a power injector. Selection of the intravenous catheter size depends on accessible venous puncture site, usually 22G—24G for younger children, 20G—22G for older children and 18G or larger for adolescents.

The peripheral venous site should be on the contralateral side of the suspected pathology to prevent streak artifact from iodinated contrast agent (e.g., right arm injection in a known left-sided aortic arch). A peripheral venous access in the leg is preferable for conditions that require assessment of any atypical venous drainage (such as after Fontan procedure or heterotaxy associated azygos continuation of an interrupted inferior vena cava) since this will ensure a homogeneous contrast enhancement in these veins and can help to avoid repeating scans due to delayed venous enhancement from post-operative anatomical changes or complications [5]. The rate of contrast injection varies and depends on the size of the angiocatheter and quality of the venous access. The routine injection rate is from 0.4 to 1.5 ml/s through a smaller gauge catheter and from 2.0 to 4.0 ml/s through a larger gauge catheter [3]. A dual power injector with saline flush is preferred over hand injection because constant contrast agent delivery results in better contrast enhancement and thus a better contrast to noise ratio [8, 9]. Bolus tracking technique is employed with the region of interest (ROI) placed within the descending thoracic aorta, at the level of the carina, and scan threshold set at 100—200 Hounsfield units (HU). Modifications on ROI placement can be done depending on the area of interest or specific CHD lesion to be evaluated. A volume of 5—20 ml of saline solution is utilized in a bolus chasing technique to dilute contrast within the right heart, prevent streak artifacts and improve contrast within the cardiac chambers.

Scan volume

CT for CHD is performed from the thoracic inlet level to L1—L2. The scan can be extended down to the lower border of the liver when there is suspicion of infracardiac anomalous pulmonary venous drainage. For a dedicated coronary CT angiography, the scan usually extends from the tracheal bifurcation to just below the diaphragm.

ECG Gating

ECG-gated image acquisition is not used routinely for younger children for the following reasons: it increases radiation dose significantly, it significantly increases scan time, which produces more respiratory artifacts; the high heart rate in infants (usually > 100 beats per minute) is too fast to prevent cardiac motion artifacts; and most of the extracardiac anatomy can be adequately depicted without ECG gating [6—10]. Even though distal coronary arteries cannot be visualized without ECG gating, non-gated CT images are sufficient to identify the origin and to evaluate the proximal course of the major arteries, which is sufficient for management of these patients [10]. For older children who can hold their breath for scanning with a heart rate of less than 80—90 beats per minute, prospective ECG-gated CT can be performed at the expense of more radiation.

Strategies for dose reduction

Reduction of the radiation exposure delivered by CT is an important issue particularly for children [3—10]. The imaging protocol should be adjusted according to the individual patient size, with every effort to minimize radiation exposure to 'as low as reasonably achievable' (ALARA) without sacrificing diagnostic image quality. The radiation dose is kept to minimum by reducing the kilovoltage (kV) and tube current (mAs) appropriately depending on the weight of the patient. In our institution, we also use iterative reconstruction algorithm (iDose4, Philips Healthcare, Cleveland, OH, USA) which helps reduce the dose but at the same time maintain image quality [11]. Other methods to reduce radiation exposure include: scan volume coverage as small as necessary; remove all metallic instruments from the chest wall if possible, particularly for scanning with automated tube current modulation; increase pitch and table speed; avoid ECG-gated acquisitions; avoid multiphase examinations; and systematic protection of nonscanned organs [1,7,8,12,13].

Image analysis

There are various image reformatting techniques used depending on target structure and purpose. These include linear or curved planar reformatting, maximum intensity projection (MIP), minimum intensity projection, shaded surface display, and volume rendering technique (VRT). The plane of the reformatted image is adjusted to correspond to the long axis of the structure of interest. Curved planar reformation is used to evaluate curved structures such as the pulmonary artery system. MIP is used mainly for evaluation of the cardiovascular structures. Minimum intensity projection is used to evaluate the airway and lung parenchyma. For three-dimensional reformatting, shaded surface display is used to evaluate the airway and lung, whereas VRT is used to evaluate the cardiovascular structures. Multiplanar reformatting (MPR) is used to better visualize and accurately measure the cardiovascular structures in question.

Discussion

CT has been used to evaluate complex CHD for more than two decades. There are many excellent comprehensive review articles on the use of cardiovascular CT for the pre- and post-operative evaluation of patients with CHD [3,8,10,13—15]. However, due to issues with radiation exposure and the possibility of adverse reaction to iodinated contrast agent, the use of CT in CHD should be reserved for situations in which it is expected to provide unique diagnostic information or less risk than other modalities. Situations in which cardiovascular CT may be appropriate in patients with CHD include the following: neonate or young patient requiring evaluation of complex anatomy, particularly if considered higher risk for adverse event with anesthesia required for cardiac MRI, and the CT scan can be performed with no or limited sedation; critically ill patient of any age that may not tolerate breath holding or length of cardiac MRI scan; patient requiring CT for evaluation of extracardiac anatomy in addition

to CHD (e.g. lung parenchyma, airway, skeletal abnormality); pre-operative patients with prior sternotomy considered high risk for vascular injury with sternal re-entry due to an anterior coronary artery, conduit, or sternal adhesions; evaluation of prosthetic valve function or structural integrity (calcification, stenosis, coaptation defect, leaflet immobility, paravalvular leak); evaluation of calcification within vessels and surgical conduits prior to catheter-based intervention (e.g. balloon angioplasty, transcatheter valve replacement, stent placement); coronary artery imaging in CHD; presence of MRI incompatible implant or foreign body (e.g., retained pacing leads, non-MRI compatible pacemaker/defibrillator, neurostimulator); poor cardiac MRI image quality due to metallic artifact; patient is unable to fit in the MRI scanner due to obesity or suffers claustrophobia; and evaluation of ventricular assist device or extracorporeal membrane oxygenation (ECMO) cannula positioning [6,7].

Cardiovascular CT plays important supplementary role in the anatomic evaluation of patients with complex CHD [1—10,12—16]. When findings with other imaging modalities are equivocal, the use of CT may help decrease diagnostic error. Although it is capable of detecting intracardiac abnormalities, CT currently does not compete with echocardiography and MRI in the evaluation of intracardiac shunts and valvular anomalies. CT is also limited in providing functional and flow information. Patients with CHD are commonly referred for CT to characterize extracardiac structures before intervention. The pulmonary arteries, pulmonary veins, coronary arteries, aortic arch and great vessels may be inadequately characterized at echocardiography, necessitating further assessment with CT.

Pulmonary arteries and systemic-to-pulmonary blood supply

The ability to reliably visualize pulmonary arterial supply is one of the strengths of cardiovascular CT. CT is an excellent imaging modality in evaluating patients with tetralogy of Fallot (TOF) or double outlet right ventricle (DORV) who are not adequately imaged by echocardiography prior to repair, particularly in those with pulmonary atresia [3,5,6]. CT can show the diminutive pulmonary arteries not demonstrated during cardiac catheterization

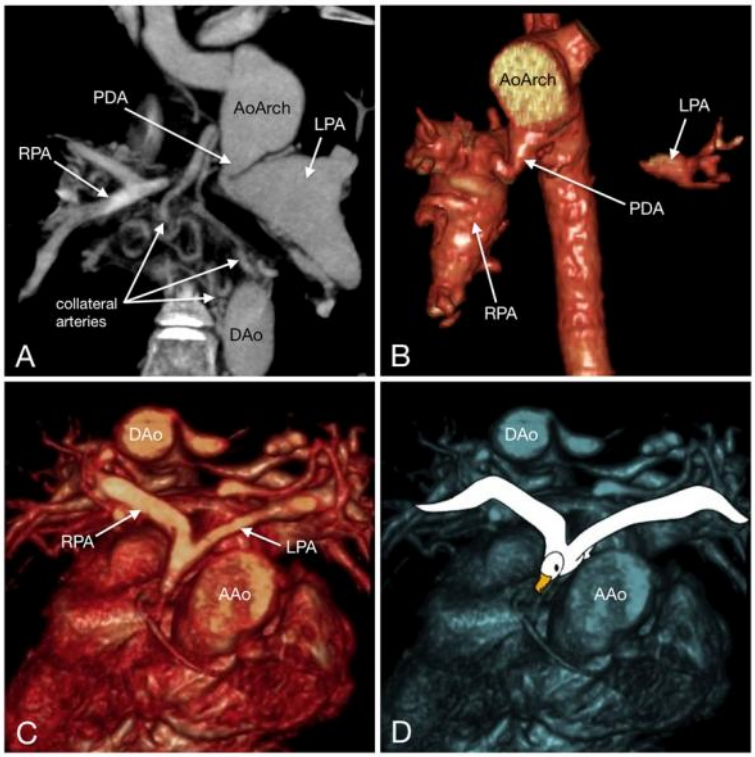

Figure 1. Pulmonary atresia with non-confluent (A and B) and confluent pulmonary arteries (C and D). MIP coronal image in A shows a PDA arising from a left-sided aorta supplying the dilated left pulmonary artery, a small right pulmonary artery, and multiple collateral arteries supplying the right lung. Volume rendered CT image in B shows a PDA arising from a right-sided aorta supplying the dilated right pulmonary artery and a diminutive floating left pulmonary artery. Volume rendered CT images in C and D showing small but confluent pulmonary arteries ("seagull sign" in D) in a 3-year-old patient with pulmonary atresia. RPA = right pulmonary artery, LPA = left pulmonary artery, PDA = patent ductus arteriosus, AAo = ascending aorta, AoArch = aortic arch, DAo = descending aorta.

[3,16]. The most important aspect of CT in evaluating patients with these cardiovascular anomalies is analysis of the pulmonary artery anatomy and anomalous pulmonary blood supply [3,5,10]. Pulmonary blood flow in patients with pulmonary atresia may be supplied via a patent ductus arteriosus (PDA), major aortopulmonary collateral arteries (MAPCAs) or both (Figure 1A and 1B). Images should be carefully analyzed for the following: length of pulmonary atresia; presence of pulmonary artery confluence; size of the pulmonary arteries at the origin and at the hilum; presence of branch pulmonary artery stenosis; and sources of pulmonary blood flow to each lung, including the number of bronchopulmonary segments supplied by native pulmonary arteries and the distribution of MAPCAs. These informations play a major role in determining the prognosis and mode of surgical treatment. On CT, the confluent pulmonary arteries, together with the abbreviated main pulmonary trunk, appear as a seagull in flight (Figure 1C and 1D). CT images provide diagnostic mapping to guide the interventionists with coil embolization and help cardiovascular thoracic surgeons plan unifocalization and staged repair.

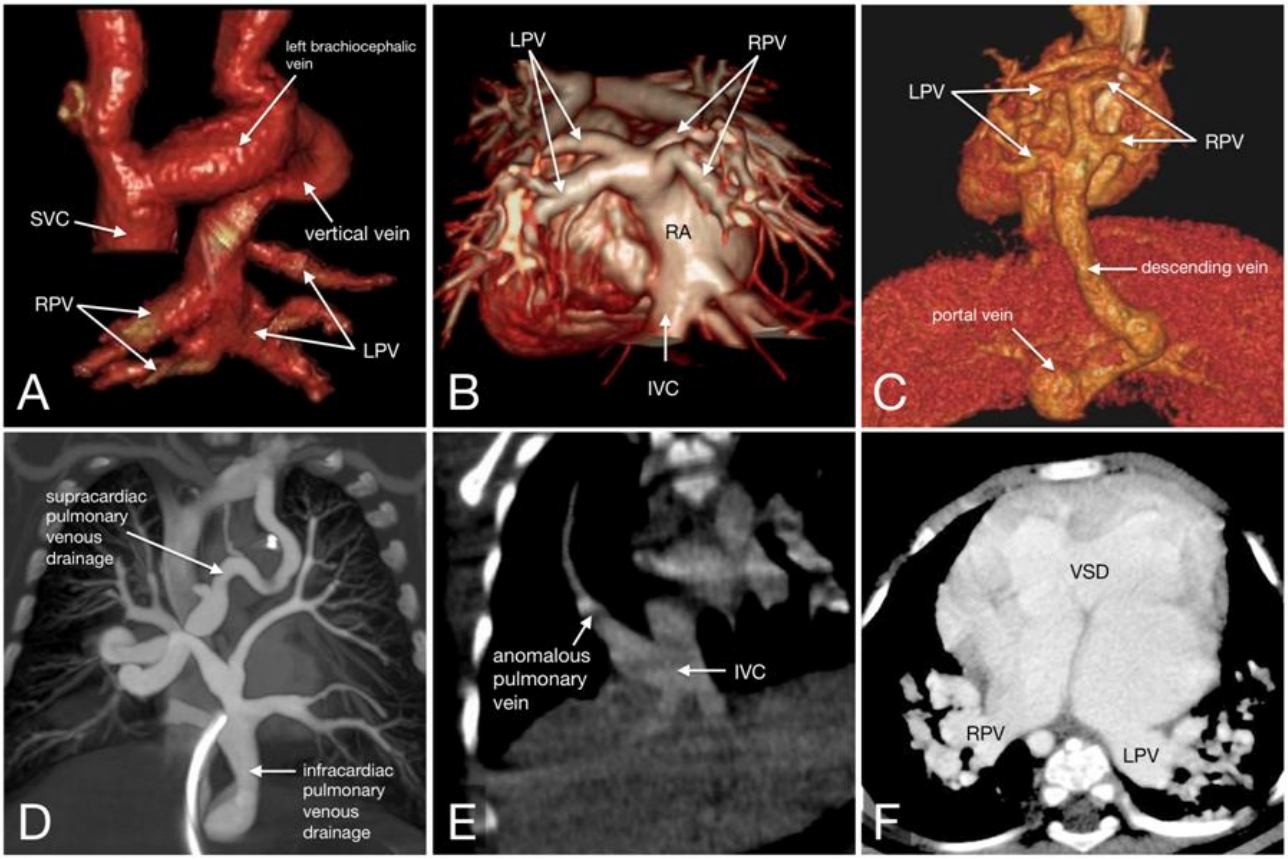

Figure 2. CT images of anomalous pulmonary venous connections. A, Volume rendered image (frontal view) of type I (supracardiac) TAPVR showing all pulmonary veins draining into the superior vena cava through the left vertical vein and left brachiocephalic vein. B, Volume rendered image (posterior view) of type II (cardiac) TAPVR with all pulmonary veins draining into the right atrium. C, Volume rendered image (posterior view) of type III (infracardiac) TAPVR revealing all pulmonary veins draining to a common venous channel, which descends and drains into the portal circulation. D, MIP coronal image of type IV (mixed) TAPVR with a combination of supracardiac and infracardiac anomalous pulmonary venous connections. E, Neonate with Scimitar syndrome showing the anomalous right lower lobe pulmonary vein draining into the inferior vena cava. F, Cyanotic infant with mesocardia, VSD and left atrial isomerism showing the right pulmonary vein draining into the right-sided atrium and the left pulmonary vein draining into the left-sided atrium. RPV = right pulmonary veins, LPV = left pulmonary veins, SVC = superior vena cava, IVC = inferior vena cava, RA = right atrium, VSD = ventricular septal defect.

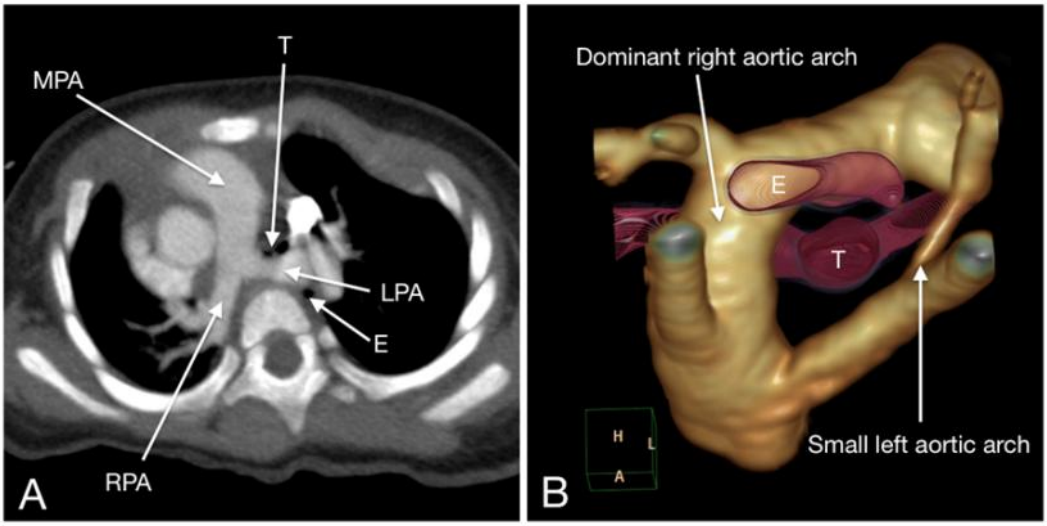

Figure 3. CT images of pulmonary sling and vascular ring. A, Axial MIP image demonstrates the aberrant left pulmonary artery (pulmonary sling) arising from the right pulmonary artery passing between the trachea and esophagus. B, Volume rendered image showing double aortic with dominant right arch and hypoplastic left arch forming a vascular ring that surrounds the trachea and esophagus. MPA = main pulmonary artery, RPA = right pulmonary artery, LPA = left pulmonary artery, T = trachea, E = esophagus.

Anomalous pulmonary venous connections

Cardiac CT is well established for the evaluation of partial and total anomalous pulmonary venous return (PAPVR and TAPVR) and conditions where pulmonary veins drain to structures other than the left atrium (Figure 2). CT can provide information on the site of abnormal venous drainage, pulmonary venous obstruction, and associated other abnormalities of the heart and lung [3,17]. Tools like 3D volume rendering and maximum intensity projections greatly aid in the understanding of the complex and tortuous vascular course.

Vascular rings, pulmonary slings and aortic arch anomalies

CT has become the preferred imaging examina-

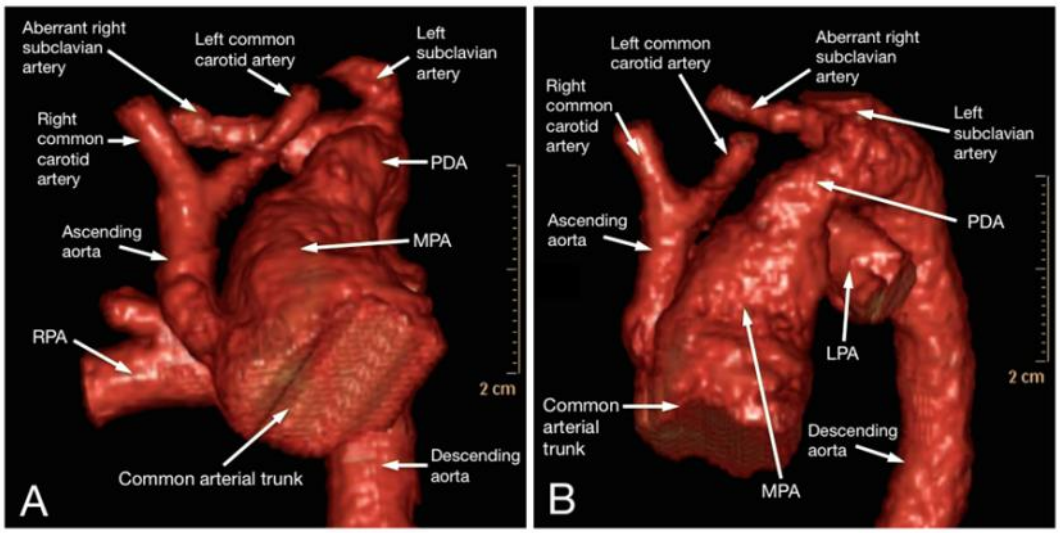

Figure 4. CT images of a cyanotic neonate with truncus arteriosus, interrupted aortic arch and aberrant right subclavian artery. Prior echocardiographic examination was only able to demonstrate truncus arteriosus and classified the anomaly as Collett and Edwards type II (Van Praagh type A2). CT was able to demonstrate a coexistent type B interrupted aortic arch with a hypoplastic ascending aorta, PDA supplying the descending aorta, and aberrant right subclavian artery. The anomaly was reclassified as Van Praagh type A4. MPA = main pulmonary artery, RPA = right pulmonary artery, LPA = left pulmonary artery, PDA = patent ductus arteriosus.

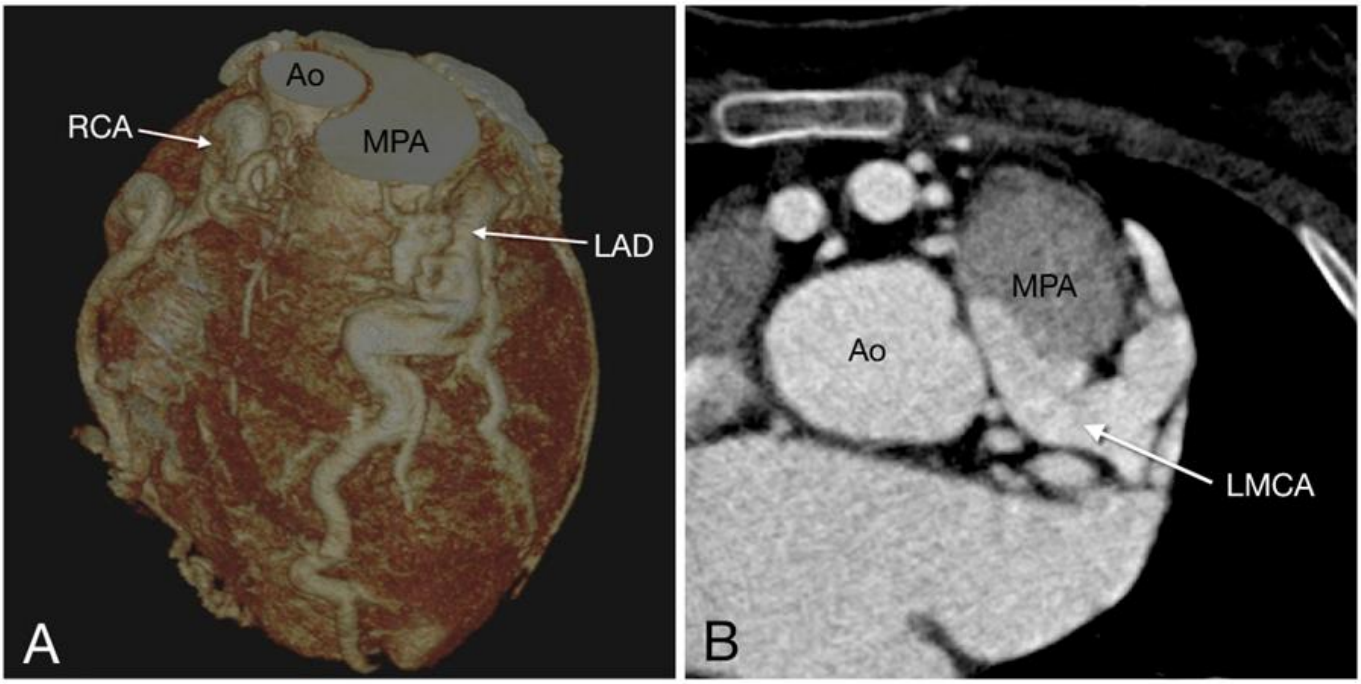

Figure 5. Coronary CT of a young patient with anomalous left coronary artery from the pulmonary artery (ALCAPA or Bland-White-Garland syndrome). Prior echocardiographic examination showed findings suspicious for coronary fistula. A, volume rendered image showing tortuous and dilated coronary arteries. B, axial image shows the left main coronary artery arising from the main pulmonary artery with reflux of contrast into the latter suggestive of reversal of flow. No significant stenosis or coronary fistula identified in this examination. Ao = aorta, MPA = main pulmonary artery, LMCA = left main coronary artery, LAD = left anterior descending coronary artery, RCA = right coronary artery.

tion for the diagnosis and characterization of vascular rings and pulmonary slings (Figure 3) because of rapid acquisitions, making it feasible to perform the study without sedation or general anesthesia. It is performed in symptomatic patients to delineate the anatomy and help surgical planning. CT provides excellent spatial and temporal resolution, a wide field of view, multiplanar reconstruction capabilities and simultaneous evaluation of the vasculature, airways and, to a lesser degree, the esophagus [18].

CT depicts the thoracic aorta noninvasively and in exquisite detail. Numerous congenital anomalies of the aorta, like coarctation and aortic arch interruption (Figure 4), can be diagnosed with this imaging technique, including anomalous arch branching patterns and configurations. CT also can be used to establish situs and L- versus D-looping of the great vessels [3]. A combination of axial, 2D reformatted, and 3D volume rendered images can be used to accurately depict these anatomic relations.

Congenital and acquired coronary artery disease

Detailed coronary artery imaging is possible in nearly every patient using a current generation CT scanner. Clinical scenarios where coronary CT imaging may be considered in children with CHD include: patients needing detailed preoperative coronary artery evaluation in addition to assessment of complex anatomy, patient with symptoms and signs suggestive of atherosclerotic coronary artery disease and a history of CHD, prior coronary intervention, or high risk Kawasaki disease, young symptomatic patients with known or suspected coronary anomaly, particularly if cardiac MRI is unlikely to provide complete assessment or more likely to require anesthesia, delineation of coronary anatomy prior to percutaneous pulmonary valve implantation, and evaluation of coronary artery after any surgery requiring coronary artery manipulation or reimplantation [6,7]. Anomalous coronary arteries are frequently associated with CHD. The most frequent anomalous find-

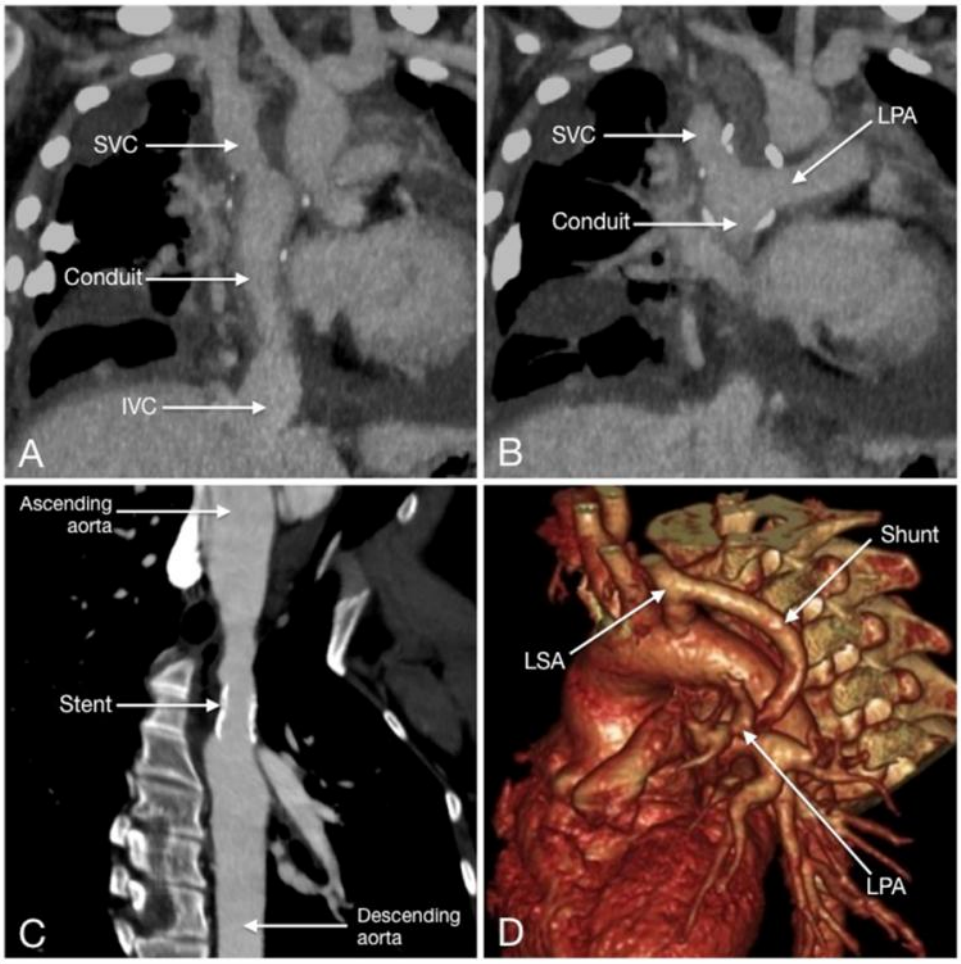

Figure 6. CT after CHD surgery and intervention. A and B, CT images demonstrating a patent conduit that connects the inferior vena cava with the pulmonary arteries and superior vena cava in a Tricuspid atresia patient who underwent Fontan procedure. Pericardial and pleural effusions are also seen. C, Curved planar reformation CT after stent implantation for aortic coarctation. D, Volume rendered image showing a left modified Blalock-Thomas-Taussig shunt (patent prosthetic graft interposed between the left subclavian artery and ipsilateral pulmonary artery) in a Tetralogy of Fallot patient. SVC = superior vena cava, IVC = inferior vena cava, LPA = left pulmonary artery, LSA = left subclavian artery.

ing is a left coronary artery originating from right coronary sinus but many variants are possible, even coronary artery originating from pulmonary arteries (Figure 5). Detection of an anomalous origin of coronaries is especially important before surgery when a ventriculotomy is planned, as accidental injury to the coronary artery crossing the right ventricle during intervention can be fatal.

Evaluation after CHD intervention or surgery

CT provides excellent visualization of stents, grafts and conduits (Figure 6). It can be used to confirm palliative shunt patency and to assess various complications, like stent occlusion, stent fracture, stent migration and separation from the vessel wall, residual vessel narrowing, and pseudoaneurysms [19]. Because it facilitates rapid comprehensive assessment of thoracic structures, CT can be used in the postoperative evaluation of CHD patients whose condition suddenly deteriorates. In this situation, CT can quickly display evidence of a variety of CHD-related complications and numerous other medical conditions, such as pulmonary embolism, pneumonia, pleural and pericardial effusion, and pneumothorax. CT can be useful before a reoperation to assess the altered anatomic features related to previous surgery [3,5,19,20].

Conclusion

CT is a supplemental imaging modality for the morphologic evaluation of complex CHD. It is essentially useful in the evaluation of vascular anomalies located outside the heart and in the assessment of postsurgical anatomy. Although the role of CT in the evaluation of pediatric CHD is limited by radiation-related anxieties and other disadvantages, there are several generally accepted clinical indications for which the benefits of imaging outweigh the risks.

References

1. Tsai IC, Chen MC, Jan SL, et al. Neonatal cardiac multidetector row CT: why and how we do it. *Pediatr Radiol* 2008; 38: 438-451.

2. Leschka S, Oechslin E, Husmann L, et al. Pre and postoperative evaluation of congenital heart disease in children and adults with 64-section CT. *RadioGraphics* 2007; 27: 829-846.

3. Dillman JR, Hernandez RJ. Role of CT in the evaluation of congenital cardiovascular disease in children. *AJR Am J Roentgenol* 2009; 192 (5): 1219-2131.

4. Goo HW. Cardiac MDCT in children: CT technology overview and interpretation. *Radiol Clin North Am* 2011; 49 (5): 997-1010.

5. Siripornpitak S, Pornkul R, Khowsathit P et al. Cardiac CT angiography in children with congenital heart disease. *Eur J Radiol* 2013; 82 (7): 1067-1082.

6. Han BK, Rigsby CK, Hlavacek A et al. Computed Tomography Imaging in Patients with Congenital Heart Disease Part I: Rationale and Utility. An Expert Consensus Document of the Society of Cardiovascular Computed Tomography (SCCT): Endorsed by the Society of Pediatric Radiology (SPR) and the North American Society of Cardiac Imaging (NASCI). *J Cardiovasc Comput Tomogr* 2015; 9 (6): 475-492.

7. Han BK, Rigsby CK, Leipsic J et al. Computed Tomography Imaging in Patients with Congenital Heart Disease, Part 2: Technical Recommendations. An Expert Consensus Document of the Society of Cardiovascular Computed Tomography (SCCT): Endorsed by the Society of Pediatric Radiology (SPR) and the North American Society of Cardiac Imaging (NASCI). *J Cardiovasc Comput Tomogr* 2015; 9 (6): 493-513.

8. Hellinger JC, Pena A, Poon M et al. Pediatric computed tomographic angiography: imaging the cardiovascular system gently. *Radiol Clin N Am* 2010; 48(2): 439-467.

9. Krishnamurthy R. Neonatal cardiac imaging. *Pediatr Radiol* 2010; 40(4): 518-527.

10. Rajeshkannan R, Moorthy S, Sreekumar KP et al. Role of 64-MDCT in evaluation of pulmonary atresia with ventricular septal defect. *AJR Am J Roentgenol* 2010; 194 (1): 110-18.

11. Kordolaimi SD, Argentos S, Mademli M et al. Effect of iDose4 iterative reconstruction algorithm on image quality and radiation exposure in prospective and retrospective electrocardiographically gated coronary computed tomographic angiography. *J Comput Assist Tomogr* 2014; 38 (6): 956-962.

12. Paterson A, Frush DP. Dose reduction in paediatric MDCT: general principles. *Clin Radiol* 2007; 62: 507-517.

13. Paul JF, Rohnean A, Sigal-Cinqualbre A. Multidetector CT for congenital heart patients: what a paediatric radiologist should know. *Pediatr Radiol* 2010; 40(6): 869-875.

14. Sigal-Cinqualbre A, Lambert V, Ronhean A, Paul JF. Role of MSCT and MRI in the diagnosis of congenital heart disease. *Arch Pediatr* 2011; 18: 617-627.

15. Crean A. Cardiovascular MR and CT in congenital heart disease. *Heart* 2007; 93: 1637-1647.

16. Greil GF, Schoebinger M, Kuettner A, et al. Imaging of aortopulmonary collateral arter-

ies with high-resolution multidetector CT. *Pediatr Radiol* 2006; 36(6): 502—509.

17. Kim TH, Kim YM, Suh Ch, et al. Helical CT angiography and three-dimensional reconstruction of total anomalous pulmonary venous connections in neonates and infants. *AJR Am J Roentgenol* 2000; 175(5): 1781-1786.

18. Etesami M, Ashwath R, Kanne J et al. Computed tomography in the evaluation of vascular rings and slings. *Insights Imaging* 2014; 5 (4): 507-521.

19. Fidler JL, Cheatham JP, Fletcher SE, et al. CT angiography of complications in pediatric patients treated with intravascular stents. *AJR Am J Roentgenol* 2000; 174: 355-359.

20. Rajiah P, Schoenhagen P. The role of computed tomography in pre-procedural planning of cardiovascular surgery and intervention. *Insights Imaging* 2013; 4 (5): 671-689.

Corresponding author :

Vincent Tatco, MD
Institute of Radiology, St. Luke's Medical Center — Global City
32nd Street corner Rizal Drive, Bonifacio Global City, Taguig City, Philippines
E-mail address: vrtatco@stluke.com.ph

Multidetector CT Scan of the Thoracic Aorta in the Evaluation of Interrupted Aortic Arch: A review

Timothy Reynold U. Lim, MD, Jacqueline Austine U. Uy, MD

Institute of Radiology, St. Luke's Medical Center, Philippines

Abstract

Interrupted aortic arch is the absence of luminal continuity between the ascending and descending portions of the thoracic aorta. It is exceedingly rare, comprising about 1-1.5% of congenital cardiovascular anomalies. The Celoria-Patton classification divides IAAs into three types depending on the site of interruption, the most common of which is type B (53-84%).

This article aims to review the types of Interrupted Aortic Arch (IAA), its Multidetector Computed Tomography scan (MDCT) angiography appearance and current imaging strategies. The pre-operative CT Angiogram findings in patients with IAA performed at our institution were also evaluated and presented in this paper. Echocardiography is the primary imaging modality in the evaluation of congenital heart disease; however CT is an important contemporary diagnostic tool. CT is particularly helpful in differentiating IAA from coarctation and other complex cardiac diseases, but it is not also without its disadvantages.

Multidetector CT scans are useful in evaluating the thoracic aorta in IAA, and also delineates the presence of collateral vessel formation, which affects the surgical treatment and prognosis of patients. The advantages of MDCT far outweigh its disadvantages when taking into account of anatomic detail, flexibility of multiplanar reconstruction, and the decreased need for sedation.

Introduction

Interrupted aortic arch (IAA) is defined as absence of luminal continuity between the ascending and descending portions of the thoracic aorta. It is an exceedingly rare condition, comprising only 1-1.5% of congenital cardiovascular anomalies [1, 2]. Its reported incidence is 0.003 per 1000 live births [3]. It usually presents with progressive heart failure symptoms of tachycardia, tachypnea, and growth impairment in neonates. If left untreated, death usually ensues after physiologic closure of the ductus arteriosus by the 4th to 10th day of life. Grayish discoloration of the lower body is the hallmark sign by this time. Significant systolic blood pressure differences may also be detected between the upper and lower extremities. Rarely, it may be diagnosed in later life and in adults if extensive collateral circulation is present between the interrupted segments [3,4,5].

IAA is usually initially managed by prostaglandin therapy to maintain ductus arteriosus patency prior to surgery, with definitive surgical management performed as soon as possible after diagnosis. The overall survival rate post-repair is around 59-85% at 16 years, which is due to improved post-operative care, surgical techniques and medical therapy [1,4,6,7].

In this article, we discuss the Multidetector CT Scan Angiography (MDCT) findings of IAA, its types, developmental anatomy, pathogenesis, important pre- and post-surgical considerations, and scanning protocols. The spectrum of CT angiogram findings of pre-operative patients with IAA in our institution seen over a ten-year period (2005 to 2015) is also presented. We re-

port a total of four cases, the youngest of which is a 1 day old female infant, and the oldest is a 17 year-old adolescent.

Interrupted Aortic Arch Types and Classification

IAA is classified according to the anatomic location of the aortic arch discontinuity, as introduced by Celoria and Patton in 1959. In type A, the interrupted segment is distal to the left subclavian artery (13-42% of cases). Type B, which is the most common worldwide (53-84%), is defined by a discontinuity between the left common carotid and the left subclavian arteries. In type C, the disruption is between the innominate artery and the left common carotid (3-4%) [1,8]. In the Korean population however, type A interrupted arch was reported to be more common than type B [9]. Each of these types may be further subclassified according to the origin of the right subclavian artery: Subtype 1 demonstrates a normal subclavian artery location, while subtype 2 shows an aberrant right subclavian artery distal to the left subclavian, and lastly, subtype 3 refers to the right subclavian artery arising from the patent ductus arteriosus [10]. Some cases of interrupted 'Right-sided' aorta have also been reported [9].

Developmental Anatomy and Pathogenesis

The aortic arch is segmentally divided into three segments: the proximal arch from the take-off of the innominate artery to the left common carotid artery, the distal arch from the left common carotid artery to the take-off of the left subclavian artery, and the isthmus which connects the distal arch to the juxtaductal descending aorta [1,3].

The thoracic aorta and its three main branches are developmentally formed from six pairs of aortic arches connecting two primitive ventral and dorsal aortas and the seventh intersegmental arteries. The ventral aortas fuse to form the ascending aorta. The left fourth aortic arch persists to form the normal left aortic arch between the left coronary artery and left subclavian artery. A portion of the left dorsal aorta persists as the distal arch and proximal descending aorta, while the cranial portion of the right dorsal aorta originates the proximal right subclavian.

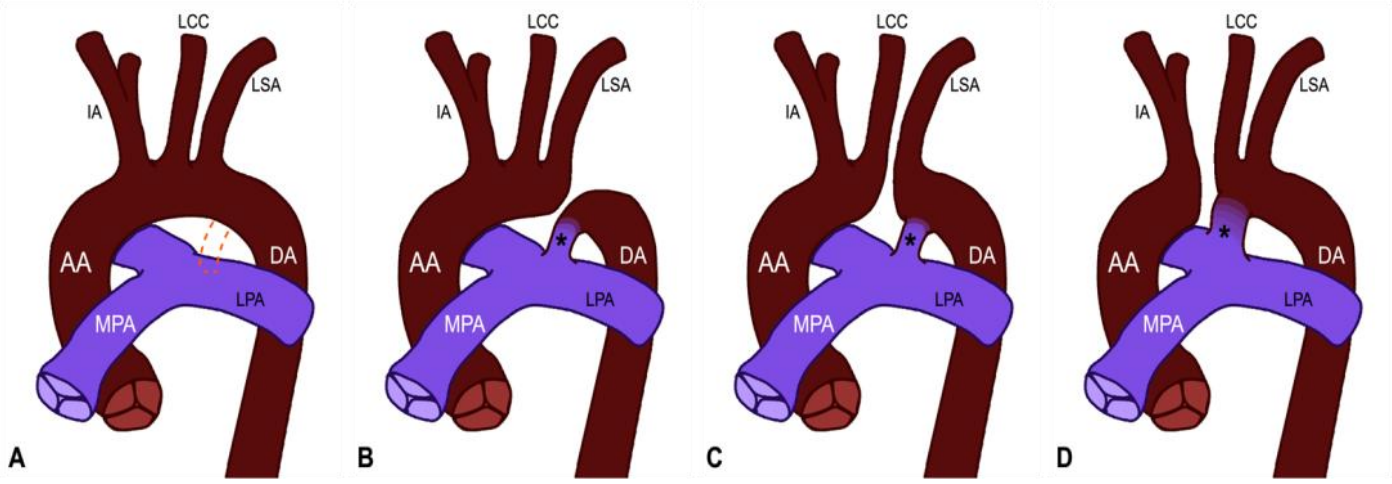

Figure 1: Schematic diagrams of the normal aortic arch configuration (A) with expected location of the ligamentum arteriosum (broken orange lines), interrupted aortic arch type A (B), type B (C) and type C (D). *(Illustration by JA Uy, MD)*

The remainder of the two dorsal aortas fuses to form a single and more distal descending thoracic aorta. The third arches give rise to the left and right common carotid arteries. The seventh intersegmental arteries migrate cephalad to form the distal right subclavian and left subclavian arteries [1,3,11].

With regards to the normal embryological development, several mechanisms have been deduced regarding the formation of IAA types. Type A IAA probably results when the left fourth arch segment abnormally regresses after ascension of the left subclavian to its normal position or when there is a regression of the segment of the left dorsal aorta between the ductus arteriosus and the left subclavian artery. On the other hand, a type B IAA is formed when the left fourth arch segment regresses earlier than the left subclavian migration. Type C IAA is caused by failure of formation of the left third and fourth aortic arches with persistence of the ductus caroticus (portion of the embryonic dorsal aorta between the third and fourth aortic arches) as the left common carotid artery. An alternative theorized mechanism is failure of connection of the aortic sac outgrowth with the third and fourth aortic arch, with fusion of the two arches to form the left common carotid artery [11,12].

The exact pathogenesis of IAA is not definitely known, and varied etiologies had been suggested. Decreased blood flow through the fourth aortic arch during embryogenesis is suggested to be a contributory factor. Teratogen exposure during intrauterine period is also suggested as causative, [2]. Underlying genetic causes such as chromosome 22q11.2 deletion seen in 50% of cases and its association with DiGeorge syndrome are also thought to be contributory [4]. DiGeorge syndrome is seen in 40-50% of patients with IAA, and conversely, 42% of patients with DiGeorge syndrome have an associated IAA [2,4].

Associated Cardiac and Extracardiac Defects

IAA rarely occurs as an isolated anomaly. It almost always co-exist with other cardiovascular malformations, the most common of which are patent ductus arteriosus (PDA) and ventricular septal defect (VSD). IAA with only PDA and VSD is termed as simple IAA [1]. A PDA is generally required to provide maintained blood flow to the descending thoracic and distal portions of the aorta beyond the interruption, and is seen in almost all cases (97%) [4-7]. A VSD is observed in about 90-92%, which is most commonly a perimembranous type that is frequently malaligned with posterior deviation of the outlet septum, which causes obstruction of the left ventricular outflow tract (LVOT) [9].

More complex forms of IAA have associated conotruncal defects such as a truncus arteriosus, transposition of the great arteries, aortopulmonary window, and double outlet right ventricle have also been reported. These generally have poorer patient prognosis due to more complex surgical repair, prolonged procedure duration and more complex arch configurations. Other reported associated anomalies include atrial septal defects, single ventricle, and aberrant right subclavian arteries.

Few extracardiac manifestations have been reported in literature, including thymic hypoplasia. The presence of the thymus is particularly important since absence or hypoplasia suggests DiGeorge syndrome. One of the cases at our institution reveals a hiatal hernia. Otherwise, there is paucity of reports regarding concomitant extracardiac findings, but these may also be attributed as manifestations of an associated

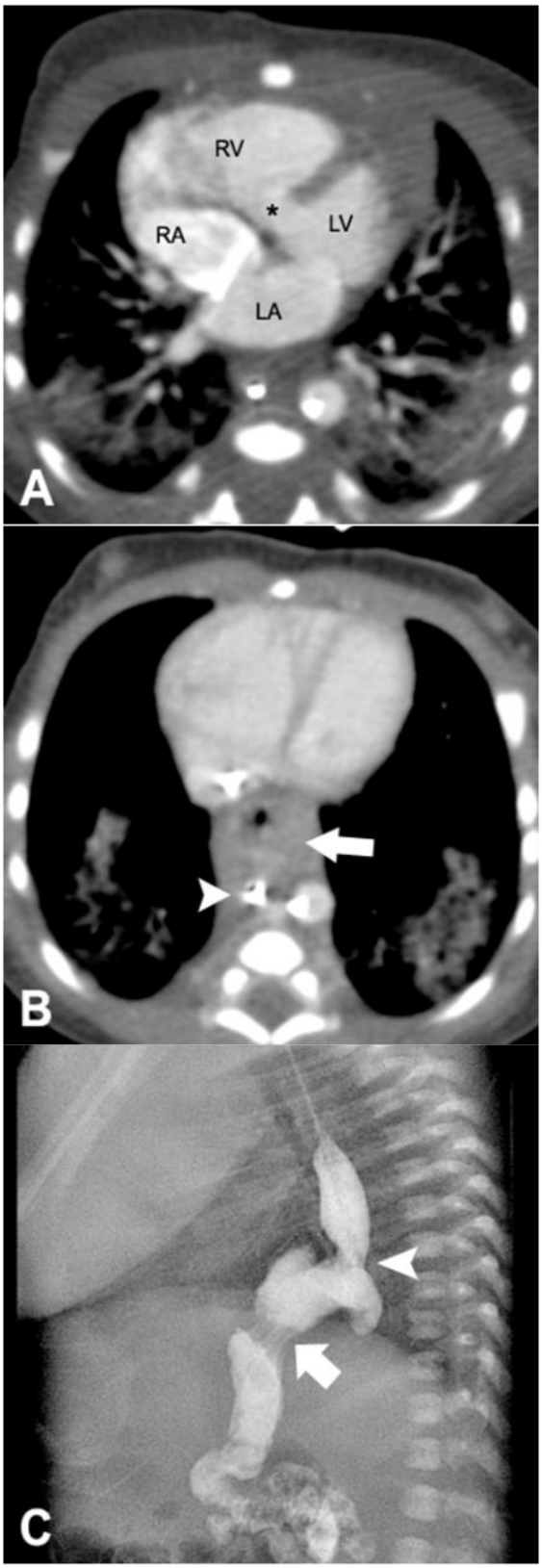

Figure 2: Associated cardiac and extracardiac defects. (A) Axial CT angiogram image from a 3-day old male infant with Type B1 IAA, showing the ventricular septal defect (asterisk). (B) Axial image on venous phase on the same patient demonstrates a retrocardiac fluid-filled structure (white arrow), with a feeding tube coursing through it (white arrowhead). (C) Lateral fluoroscopic image with water-soluble contrast injected through the feeding tube shows intrathoracic location of the gastroesophageal junction (white arrowhead) including the gastric fundus and cardia. Constriction of the proximal body (white arrow) at the level of the esophageal hiatus is also noted. These findings confirm the presence of a hiatal hernia.

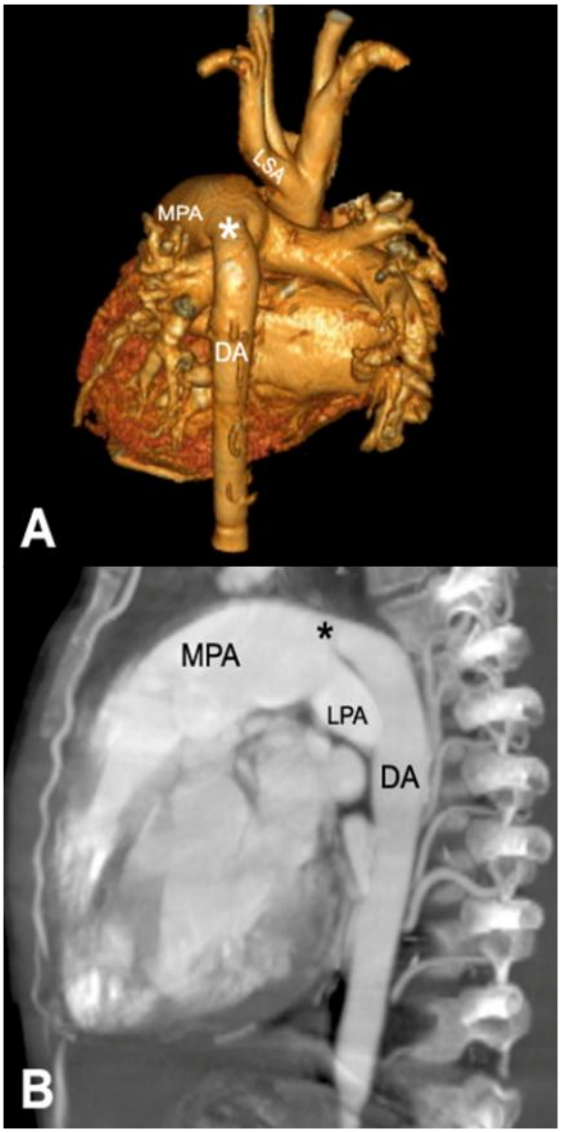

Figure 3: 11 year old female without previous surgical intervention, diagnosed to have IAA type A1. Volume-rendered reconstruction (A) shows interruption of the aortic arch distal to the left subclavian artery (LSA). The main pulmonary artery (MPA) continues into the descending aorta (DA) through a patent ductus arteriosus (white asterisk). Sagittal maximum-intensity projection image (B) again delineates the patent ductus arteriosus (black asterisk) serving as a conduit between the heart and systemic circulation. Prominent intercostal vessels are also noted. The subclavian arteries of this patient were normal in caliber and without aberrant course, hence its A1 subtype.

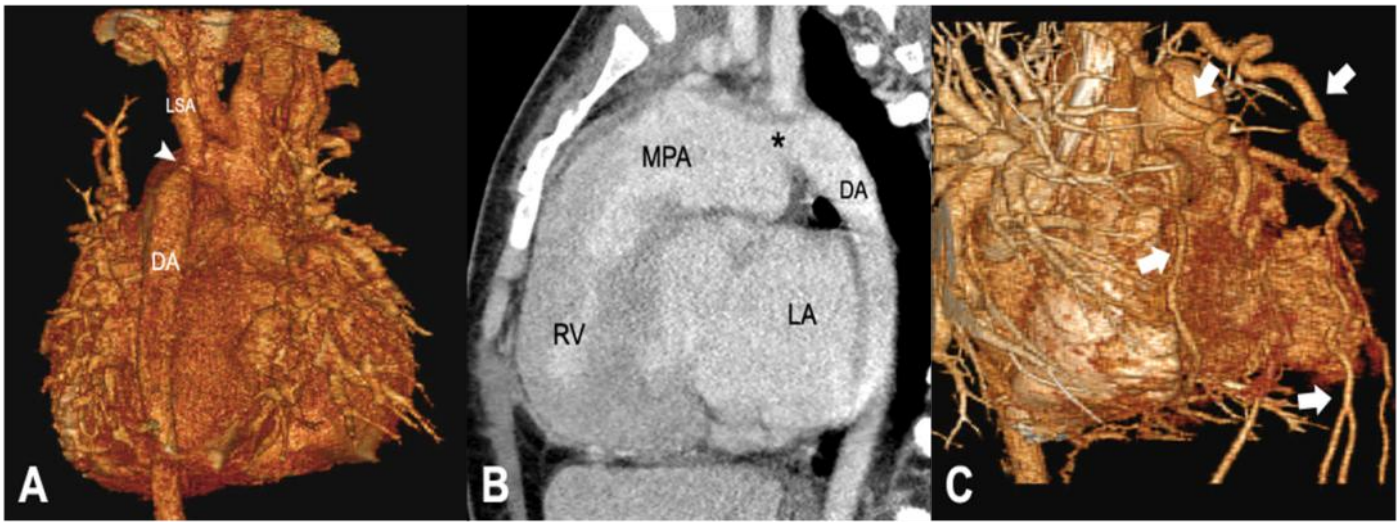

Figure 4: 17 year old female with prior history of VSD closure. The patient was referred for CT scan because of hypertension and discrepancy between blood pressures of the upper and lower extremities. The IAA was not identified prior to this examination. Volume-rendered reconstructed image (A) shows a globularly enlarged heart with interrupted aortic arch (white arrowhead) distal to the left subclavian artery (LSA). Sagittal contrast-enhanced image (B) shows the communication (asterisk) between the main pulmonary artery (MPA) and the distal aorta (DA). There is right ventricular (RV) hypertrophy producing narrowing of the ventricular outflow tract. Another volume-rendered image (C) shows prominent intercostal arteries and collateral vessel formation (white arrows).

chromosomal disorder.

The Role of MDCT and CT Angiography (CTA)

Although echocardiography still remains the primary and initial imaging modality in evaluating congenital heart disease and in diagnosing IAA, CTA is an important complementary diagnostic tool, alongside Magnetic Resonance Imaging (MRI) [2]. Echocardiography is highly operator dependent and is limited in its ability to evaluate extracardiac and complex vascular anomalies due to acoustic window limitations. Differentiating IAA from severe coarctation of the aorta and a hypoplastic arch is also be difficult with echocardiography [1,2]. CTA is more helpful in differentiating IAA from hypoplasia/atresia and coarctation. Presence of continuity between the ascending and descending aorta through an imperforate fibrous strand may signify aortic atresia, while marked dilation of the proximal descending aorta points towards the diagnosis of coarctation, which are depicted well on CT and not on echocardiography.

The advantages of CTA over other modalities such as conventional angiography and MRI include shorter scanning time, minimization of motion artifacts, reduced need for sedation, high temporal and spatial resolution, better delineation of major vascular collaterals, as well as simultaneous evaluation of the airways and lung parenchyma. However, CT scanning is associated with increased radiation dose and requires intravenous contrast administration which poses additional risks, especially for pediatric patients [2,9].

With the advent of more advanced multidetector scanners, software development, and ability to generate multiplanar reformatted and 3D reconstructed images, CT scan has become the imaging study of choice compared to conventional angiography. This better delineates complex arch morphology and other anomalies, including better understanding of the anatomic relationships to aid clinicians in deciding treatment options.

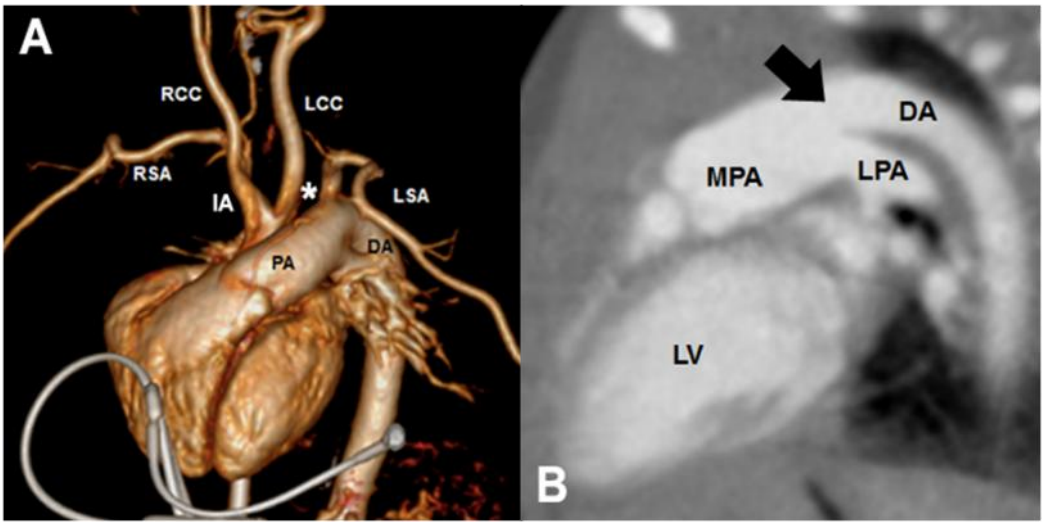

Figure 5: 3 day-old male infant with Interrupted Aortic Arch Type B1. Volume-rendered reconstruction (A) shows the area of interruption (asterisk) between the left common carotid artery (LCC) and the left subclavian artery (LSA). Note the normal origin of the right subclavian artery (RSA). The LSA emanates from the proximal descending aorta (DA). Sagittal reformatted contrast-enhanced image of the same patient (B) shows communication of the proximal descending aorta (DA) via a patent ductus arteriosus (black arrow) with the main pulmonary artery (MPA). Other structures identified are the right common carotid artery (RCC), innominate artery (IA), left pulmonary artery (LPA) and the left ventricle (LV).

Pre-operative and Post-operative Evaluation of IAA using CTA

Importance of Pre-operative CT Scans

Prompt surgical management is usually needed after the diagnosis, which may be made by either a two stage or single stage repair [13]. The preferred surgical option is a single stage procedure with simultaneous repair of the IAA and patch closure of the VSD with cardiopulmonary bypass, particularly in cases of simple IAA with only PDA and VSD as associated defects. The aortic arch is usually reconstructed with an end-to-side anastomosis between the descending and ascending aortic segments. It may also be done as a two-stage approach, with primary IAA reconstruction and pulmonary artery (PA) banding, followed by eventual removal of the PA band, VSD repair, and reconstruction of the pulmonary artery, as needed [6,7]. Cases with more complex anomalies such as significant multiple VSDs, and concomitant neurological disorders and multi-organ failure usually require two-stage repair. The repair of such complex anomalies is risky, and is associated with higher early mortality [4,9].

MDCT Angiography provides accurate pre-operative and post-operative evaluation of complex cardiovascular lesions. It provides detailed images of the thoracic aorta and provides accurate measurement of the diameter of the different segments of the thoracic aorta [2]. Radiologists must be able to describe the following pre-operative features which are important for the surgeons: exact IAA type/subtype, the distance between the proximal and distal aortic segments (intersegmental distance), the narrowest dimension of the LVOT, size of the aorta, the presence of collateral vessels, and other combined cardiovascular malformations. A longer intersegmental distance may require mobilization of the descending aorta or use of interposition graft. CT also confirms the PDA size, shows tortuous course and bilaterality in rare cases [6-7,9]. In addition, mapping of anatomy and major collat-

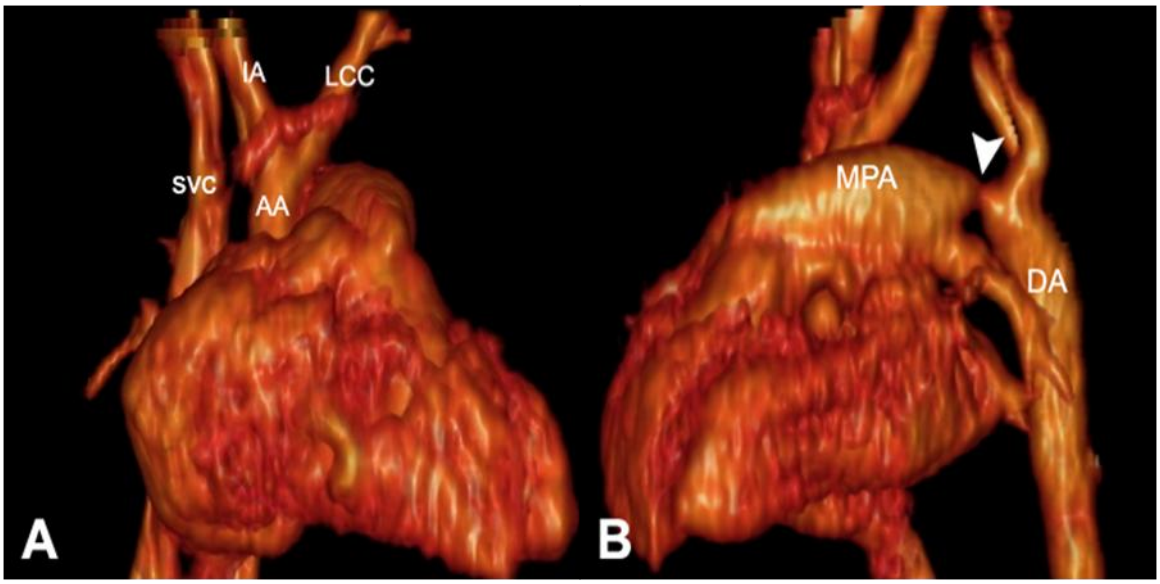

Figure 6: 1 day old female infant suspected of having aortic coarctation. CT Angiography revealed instead an IAA type B. Volume-rendered reconstruction (A and B) shows non-communication of the small ascending aorta (AA) with the descending aorta (DA) distal to the left common carotid artery (LCC). A patent ductus arteriosus is seen (white arrowhead) connecting the main pulmonary artery (MPA) and the descending aorta (DA), but it is severely narrowed of approximately 20%. The patient was given medical therapy and underwent repair at the 5th day of life.

eral vessels can aid surgeons to access the pulmonary vascular bed, minimize cardiac bypass times, and avoid tracheobronchial tree dissection [14].

CT Angiography Protocols

Various protocols regarding CT Angiography have been published, one of which is detailed by Siegel [15] and this is often modified by several centers such as ours. Intravenous contrast material is usually injected through a peripheral catheter, given at a dose of 1-2 mL/kg. At our institution, we use nonionic contrast material, and iso-osmolar nonionic contrast is preferred for hemodynamically unstable patients. Contrast may be administered via power injector or manual injection, and flow rates vary with the size of the intravenous catheters [15]. For neonates, a minimum catheter size of 24-gauge may be used. Power injector delivery can be done as long as there is proper positioning of the catheter, with adequate backflow and non-resistance upon testing, and this has been successfully performed at our center. As little as 5-8 mL of contrast is adequate for CT angiography, with successful scanning aided by the automated tracking system.

Sedation must be done for the youngest of patients. Older children and adolescents need not to be sedated since they are able to follow instructions. Several technical parameters are selected prior to scanning, and are dependent on the default manufacturer settings. At our institution, we utilize Philips Brilliance 64-Slice and iCT 256-Slice scanners for CT angiography. Collimation thickness varies between machines; however the default collimation is set as 0.625mm for both of our scanners. Other parameters include rotation time of 0.75 to 1 second, and minimum 1 x 1 mm slice thickness.

Radiation exposure is of concern to Radiologists, and also to the well-informed parent. Children are more radiosensitive relative to adults to the same dose, thus a scan that is performed should give the best image quality for the lowest possible radiation exposure [15]. Keep-

ing these rationalizations in mind, the plain/non-contrast scan could be eliminated entirely, and multiphasic studies are performed only as necessary. The settings for milliamperage (mA) and kilovoltage (kVp) are also adjusted accordingly. CT scans are performed with the lowest possible mA that produces a diagnostic quality but must also limit the radiation exposure. Kilovoltage is similarly lowered, which potentially decreases the radiation dose. Protocols may differ regarding mA and kVp among institutions, although it has widespread practice that in patients with smaller body habitus, a kilovoltage of 80 kV is adequate. Compared to the standard 120 kV protocol, using the 80 kV setting lowers radiation dose by 30 percent [15]. With regards to milliamperage settings, our protocol regarding CT angiography also follows that of Siegel [15], which is based on weight. Iterative reconstruction process is also applied which improves image quality with less radiation utilized. Post-processing such as multiplanar reconstructions and 3D volume rendering are also performed, which not only guide the cardiothoracic surgeons but also serve as a medium of instruction to relatives during pre- and post-operative family conferences.

Post-operative Scanning Considerations

Post-operative complications such as stenosis and aneurysm formation at the repair site may also be evaluated with CTA. Extrinsic bronchial compression which can cause persistent atelectasis or air trapping may also be observed as a consequence of excess anastomotic tension resulting from inadequate mobilization of the aortic segments. The left main bronchus is affected in particular since it passes under the aortic arch [13]. Contrast-enhanced CT scans are helpful in assessing patency of the surgical conduits and intravascular stents; wherein filling defects may suggest thrombosis [2,6,7]. Subaortic obstruction and aortic stenosis after surgery occurs in 50% of patients with IAA and VSD. Long term follow up with CTA is not routinely done due to prolonged radiation exposure [3,9].

Other potential complications include but are not limited to recurrent laryngeal nerve injury, chylothorax, risk for cardiac arrest and intracranial hemorrhage. These however are nonspecific, are general risks for thoracic surgery and not to IAA repair alone [9].

Conclusion

Although echocardiography is the initial imaging modality in the evaluation of congenital cardiovascular disease, MDCT Angiography remains to be the most useful complementary diagnostic imaging modality in patients with IAA. CT is particularly helpful in differentiating IAA from coarctation, associated cardiac defects, in ruling-out other complex cardiac diseases, as well as delineating extracardiac morphology. The pre-operative CT scan outlines the presence of collateral vessel formation and other associated defects, which affects the surgical treatment and prognosis of patients. Although not without its risks, the advantages of MDCT far outweighs its disadvantages when taking into account of anatomic detail, flexibility of multiplanar reconstruction, and the decreased need for sedation.

References

1. Kimura-Hayama E, Melendez G, Mendizabal A, Meave-Gonzalez A, Zambrana G, Corona-Villalobos C. Uncommon Congenital and Acquired Aortic Diseases: Role of Multide-

tector CT Angiography1. RadioGraphics. 2010;30(1):79-98.
2. Dillman J, Yarram S, D'Amico A, Hernandez R. Interrupted Aortic Arch: Spectrum of MRI Findings. American Journal of Roentgenology. 2008;190(6):1467-1474.
3. Restrepo C, Melendez-Ramirez G, Kimura-Hayama E. Multidetector Computed Tomography of Congenital Anomalies of the Thoracic Aorta. Seminars in Ultrasound, CT and MRI. 2012;33(3):191-206.
4. Frank L, Dillman J, Parish V, Mueller G, Kazerooni E, Bell A et al. Cardiovascular MR Imaging of Conotruncal Anomalies 1. RadioGraphics. 2010;30(4):1069-1094.
5. Shirani S, Soleymanzadeh M. Diagnosis of aortic interruption by CT angiography. Pol J Radiol. 2013;78(1):72-74.
6. Gaca A, Jaggers J, Dudley L, Bisset G. Repair of Congenital Heart Disease: A Primer — Part 1. Radiology. 2008;247(3):617-631.
7. Gaca A, Jaggers J, Dudley L, Bisset G. Repair of Congenital Heart Disease: A Primer — Part 2. Radiology. 2008;248(1):44-60.
8. Celoria GC, Patton RB. Congenital absence of the aortic arch. Am J Cardiol 1959;58:407-413.
9. Yang D, Goo H, Seo D, Yun T, Park J, Park I et al. Multislice CT angiography of interrupted aortic arch. Pediatr Radiol. 2007;38(1):89-100.
10. Goo H, Park I, Ko J, Kim Y, Seo D, Yun T et al. CT of Congenital Heart Disease: Normal Anatomy and Typical Pathologic Conditions1. RadioGraphics. 2003;23:147-165.
11. Reardon M, Hallman G, Cooley D. Interrupted Aortic Arch: Brief Review and Summary of an Eighteen-Year Experience. Tex Heart Inst J. 1984;11(3):250-259.
12. Roberts W, Morrow A, Braunwald E. Complete Interruption of the Aortic Arch. Circulation. 1962;26:39-59.
13. Corno AF, Festa P. Aortic Arch Interruption. In: Congenital heart defects. Decision Making for Surgery [Internet]. Darmstadt: Steinkopff-Verlag Heidelberg Publisher; 2009. [cited 2015 December 1].
14. Haramati L, Glickstein J, Issenberg H, Haramati N, Crooke G. MR Imaging and CT of Vascular Anomalies and Connections in Patients with Congenital Heart Disease: Significance in Surgical Planning1. RadioGraphics. 2002;22(2):337-349.
15. Siegel M. Multiplanar and Three-dimensional Multidetector Row CT of Thoracic Vessels and Airways in the Pediatric Population1. Radiology. 2003;229(3):641-650.

Corresponding Author:

Timothy Reynold U. Lim, MD
St. Luke's Medical Center — Quezon City
Ground Floor, X-Ray Department
279 E. Rodriguez Sr. Avenue,
Quezon City, NCR, Philippines
Email: lim.tru@gmail.com
Phone: +63 (02) 7230101, local 5417

Dengue: Multi-organ clinical correlation with Multi-modality Imaging

Mariaem M. Andres[1,2], Nathan David P. Concepcion[1,2] and Abigail L. Pomobi[1]

St. Luke's Medical Center, Quezon City[1] and Global City[2], Philippines

Abstract

Dengue is an important public health concern that is prevalent worldwide. This review article discusses the virus, pathophysiology, multi-organ clinical presentation, and multi-modality imaging approaches. The common radiologic findings encountered in the central nervous system, cardiovascular, gastrointestinal, pulmonary and musculoskeletal systems provide important diagnostic points that define the spectrum of expected imaging features of the disease.

Introduction

Dengue infection is recognized as one of the world's emerging infectious disease of public health concern. World Health Organization (WHO) reports that the incidence of dengue has grown dramatically around the world. Over 40% of the world's population (~2.5 billion) are now at risk from dengue. A current estimate of 50-100 million dengue infections worldwide occur annually and about 200,000-500,000 of these contract dengue hemorrhagic fever (DHF). Mortality is about 5%, with most numbers occurring in children less than 15 years old.

Dengue Virus, Pathophysiology and Clinical Correlation

Dengue virus (DENV) is a flavivirus, a positive-stranded enveloped RNA virus subgrouped into serotypes 1 to 4 [2,3,4]. The National Institute of Allergy and Infectious Diseases (NIAID) have classified DENV as a category A priority bio-threat pathogen meaning the virus poses the highest risk to national security and public health because it is disseminated easily, results in high mortality, and requires public health preparedness. DENV is in the same category as the Ebola virus in Africa [5]. DENV is transmitted to humans by anthropophilic mosquitoes, particularly Aedes aegypti [6,7]. In the last quarter of 2013 in Sarawak, Malaysia, a new emergence of sylvatic (non-human primates) dengue virus was noted which may represent a 5th serotype of dengue.

The disease begins on the day of inoculation of the DENV by the mosquito with an incubation period of 3-7 days [8]. The characteristic symptoms are a sudden-onset fever, headache, retro-orbital pains, muscle and joint pains and rashes [9]. The course of infection is divided into three phases: (1) febrile phase, where there is high fever that is usually bi-phasic but could also have a variable pattern; (2) critical phase, in which the patient manifests with thrombocytopenia (platelet count < 100 x 109/L) and hemoconcentration (increase in hematocrit > 20% above the average for age and sex) as well as pleural effusions and ascites due to increased capillary permeability and plasma leakage; and (3) recovery phase, where fluid gets resorbed back into the intravascular space [8,9,10].

In 2009, WHO re-classified dengue as: (1) dengue without warning signs, (2) dengue with warning signs, and (3) severe dengue. Warning signs include persistent vomiting, abdominal pain, lethargy, irritability, postural hypotension, and olig-

uria.

Infection with any one serotype confers lifelong immunity to that serotype but only two- to three -months' immunity to other serotypes. Infection with another serotype or multiple serotypes leads to more severe forms of dengue [4,11] due to Antibody-Dependent Enhancement [12,13] which incites multiple cytokine cascades which increase the permeability of the endothelial cells, most notably at the pleural and parietal endothelial cells [3,11,12].

Central Nervous System

The neurological manifestations of dengue infection is diverse, altered consciousness being the most frequent [14]. CNS involvement is seen in 4 to 50% of dengue infections [14,15,16].

There are two hypotheses explaining the neuropathogenic mechanism of dengue:

1. Direct involvement of the CNS through neurotropism that leads to encephalitis, meningitis, or myelitis
2. Secondary involvement through systemic or multi-organ derangement that leads to encephalopathy, ischemia or stroke, or hypokalaemic paralysis

Computed Tomography (CT) and Magnetic Resonance Imaging (MRI) neuroimaging findings are also diverse from normal to non-specific cerebral and spinal cord oedema. The watershed areas in the fronto-parietal lobes [16] are prone to ischemia and infarction. Wasay and colleagues have reported generalized cerebral edema and focal abnormalities in the globus pallidi, hippocampi, thalami and internal capsules. There may also be haemorrhage. Cervical and thoracic spinal cord may also occur. Lesions are usually hyperintense on T2W [17,18]. Findings in the brain can likewise mimic acute disseminated encephalomyelitis (ADEM).

Pulmonary System

Lungs of dengue patients contain viral replication products in pneumocytes and pulmonary vascular endothelium which explain the radiological manifestations of pulmonary edema, hemorrhage, infiltrates and pleural effusions

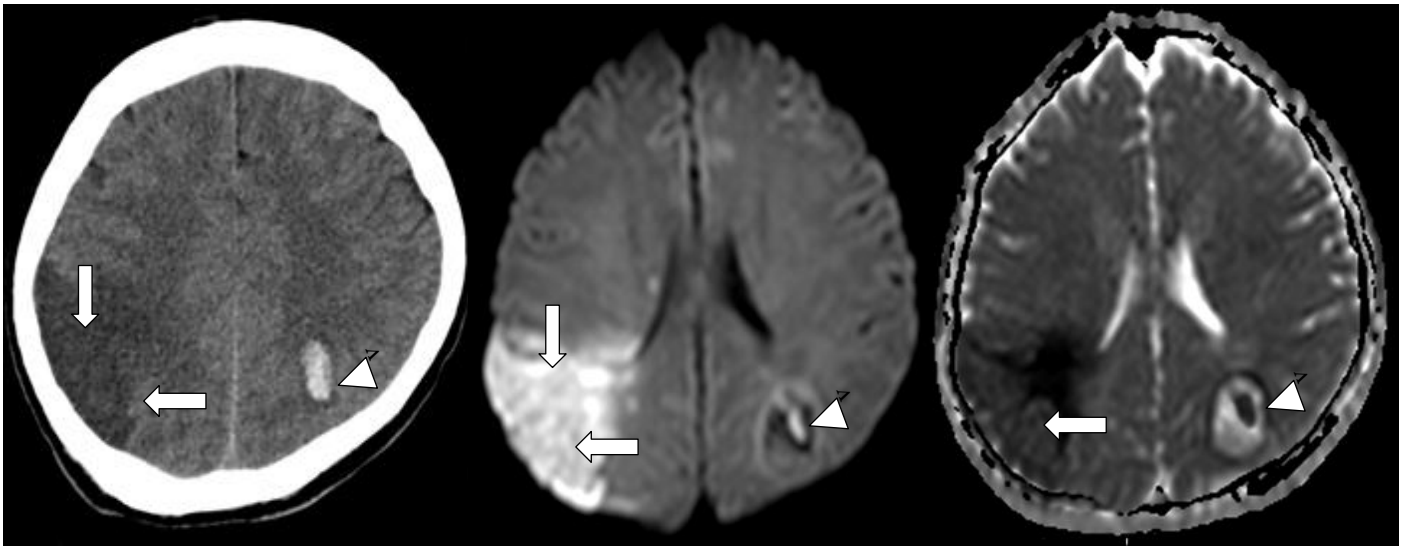

Figure 1. Neuroimaging of a 29 year-old female with dengue infection showing wedge-shaped acute infarct at the right parietal lobe (arrows) with a focal hemorrhage at the left parietal lobe (arrowheads). A, unenhanced CT scan. B, DWI. C, ADC. Magnetic resonance angiography (MRA) was unremarkable.

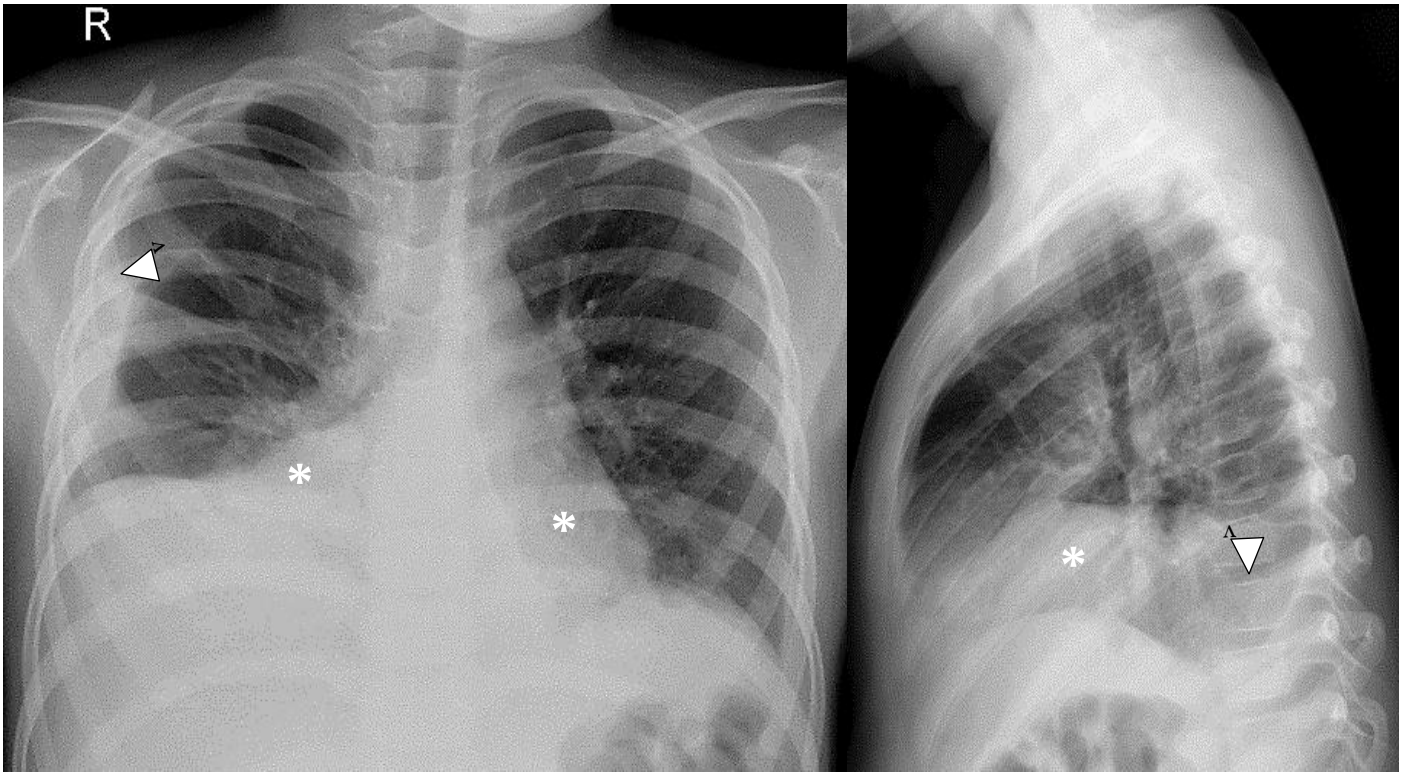

Figure 2. A 6-year old male with dengue hemorrhagic fever presenting with minimal right-sided pleural effusion (arrowheads) with parenchymal densities (asterisks) attributed to atelectasis and/or infiltarates.

[26,27,28]. Pleural effusions are the major pulmonary presentation of dengue [27,28] expected in the critical phase of the disease when plasma leakage occurs. The size of the effusions correlate with the decrease in platelet count.

Clinical and radiological differentiation between pulmonary manifestations of dengue and other infections associated with infiltrates, hemorrhage, or effusion is difficult, even in endemic regions. Physicians and radiologists need prudent consideration of other diagnostic possibilities. Serology confirms the diagnosis of dengue.

Cardiovascular System

Only limited literature describes the cardiovascular involvement of dengue which is usually asymptomatic. The underlying pathogenesis of the cardiac manifestations is explained by two theories: (1) direct viral infection of the cardiac cells, and (2) indirect effects of the inflammatory cytokine cascade [19].

Cardiac manifestations can be divided into functional impairment, arrhythmias, and myocarditis which are all transient and do not contribute to long term sequelae and are demonstrated by 2D echocardiography and MRI20. Tachycardia and bradycardia are also common. Seldom do patients with dengue receive cardiac imaging assessment, hence the detection of subclinical cardiac involvement and its effect in the overall hemodynamic instability in severe dengue remains poorly described in the literature.

Abdominal Involvement

Abdominal pain is commonest abdominal symptom in dengue and is highly non-specific [21,22] but is one of the warning signs that serves as a predictor of disease progression. A variety of solid organs can be affected, particularly the liver, pancreas, and kidneys and ascites is also described.

In children hepatomegaly occurs in 80-100% of

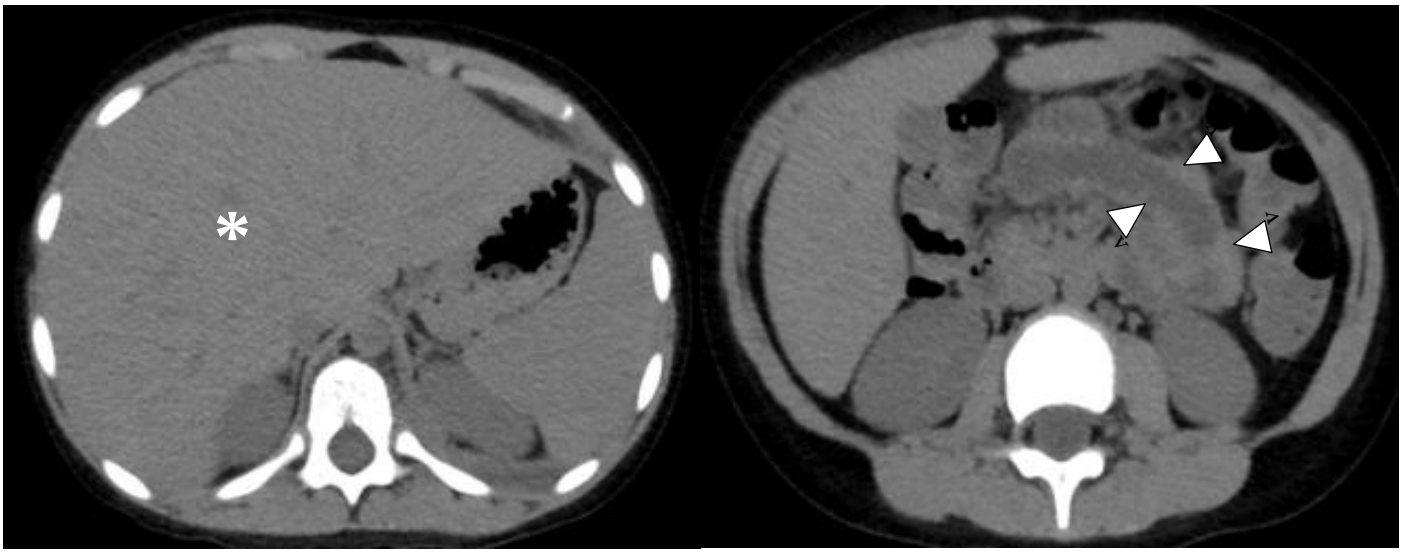

Figure 3. Axial CT scan of an 8-year old boy with dengue infection showing hepatomegaly (A, asterisk) and focal jejunal wall thickening (B, arrowheads).

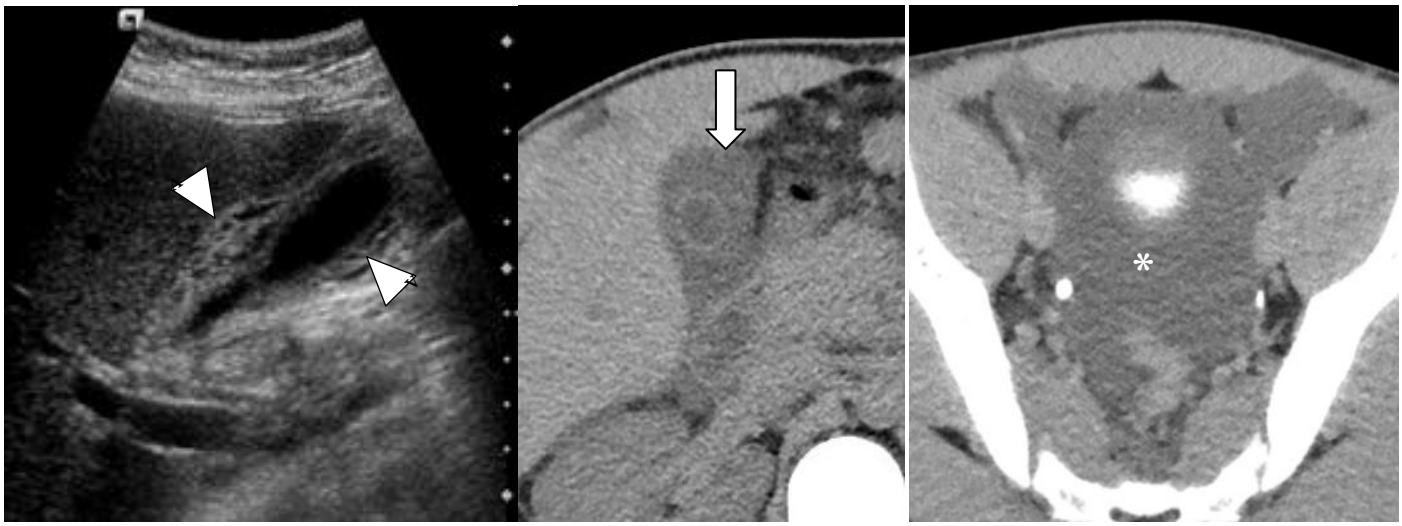

Figure 4. A, A 12-year old female with dengue fever complaining of abdominal pain. Ultrasonography reveals a 7 mm thick and oedematous gallbladder wall (arrowheads). B-C, CT scan of a 15-year old male also with dengue fever showing gallbladder wall oedema (arrow) and pelvic ascites (asterisk).

cases [23]. The injury to the liver ranges from mild hepatic dysfunction exhibited as enzyme elevation to fulminant hepatic failure. The gallbladder may present with wall thickening (> 3 mm) in 75.9% according to Reddy and colleagues [25]. A wall thickness of more than 5 mm could also be seen as a criterion for identifying dengue hemorrhagic fever (DHF) that sets the patient at high risk for developing hypovolemic shock [23, 24]. Ascites can be found in 56.7% of cases and is more common in patients with severe dengue [25].

Muscular Involvement

Muscle involvement presents with myalgia or muscle pain and occurs in almost 93% of cases [29,30,31]. Myalgia may be attributed to diffuse viral invasion of muscle and subsequent inflammatory changes.

Intramuscular haemorrhage is a very rare manifestation of dengue. A case report by Kosh, et al [30], documented spontaneous hematoma involving both iliacus muscles. However, a very rare case of uncontrolled intramuscular hemorrhage after caesarean section in a mother diagnosed

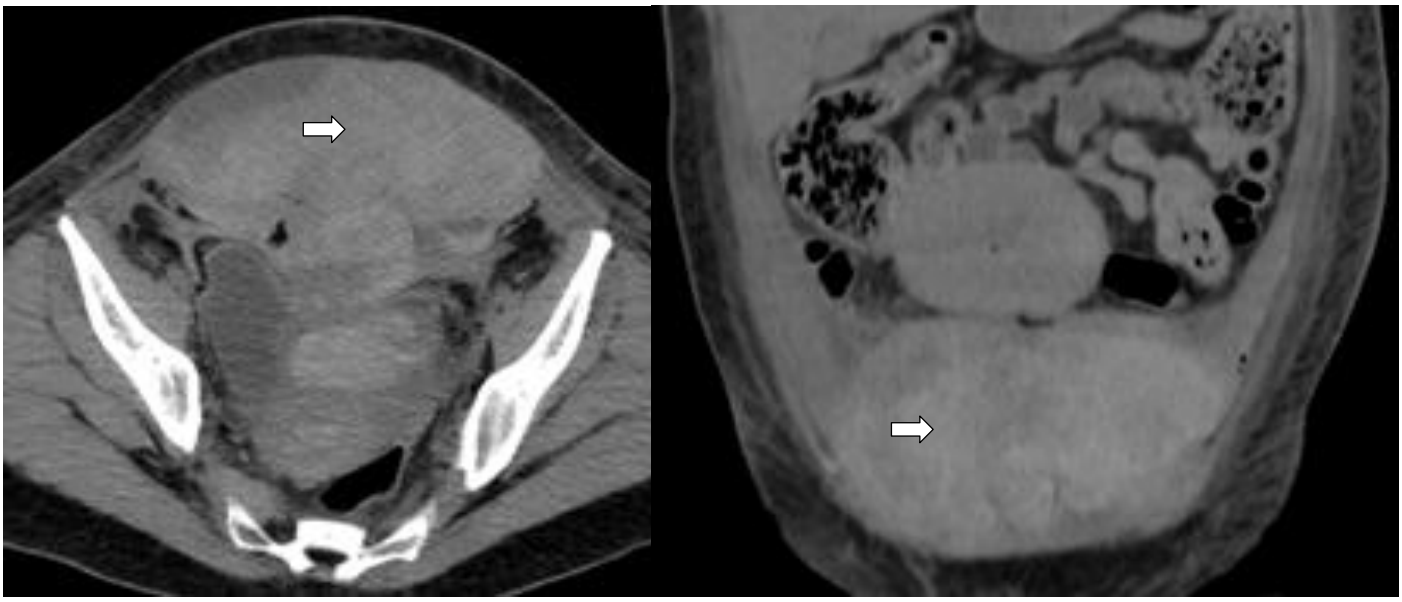

Figure 5. Voluminous acute intramuscular bleed (arrow) a day after caesarean section is detected in a 36-year old patient diagnosed with dengue.

with dengue has been described (Figure 5).

Conclusion

Dengue is one of the most common mosquito-borne viral diseases with public health significance worldwide. Increased vascular permeability that leads to plasma leakage is the pathogenic hallmark of this disease. The interplay of different factors among virus, vector, host, and immunological mechanisms contribute to clinical characteristics, disease progression and involvement of multiple organs. Radiologic imaging is important in the monitoring of the disease, and where appropriate, promotes timely intervention.

Update

The first dengue vaccine manufactured by Sanofi Pasteur was released to three (3) countries namely Brazil, Mexico, and Philippines last December 2015. The vaccine, Dengvaxia (CYTDV), is a live recombinant tetravalent vaccine given as three doses on a 0/6/12-month schedule in Phase III clinical trials. This can be administered to patients aged 9-45 years old who are living in endemic areas.

References

1. Dengue Fever World Health Organization Fact Sheet No.117, Last updated February 2015. [http://www.who.int/mediacentre/factsheets/fs117]
2. Chuang YC, Wang SY, Lin YS, et al. Re-evaluation of the Pathogenetic Roles of Non-structural Protein 1 and its Antibodies during Dengue Virus Infection. J of Biomedical Science 2013; 20.
3. Chuansumrit A and Tangnararatchakit K. Pathophysiology and Management of Dengue Hemorrhagic Fever. Transfusion Alternative in Transfusion Medicine 2006; 8 (Suppl, 1): 3-11.
4. Dash AP, Bhatia R, and Kalra NL. Dengue in South-East Asia: an appraisal of case management and vector control. In World Health Organization Dengue Bulletin, De-

cember 2012; 36: 1-13.

5. National Institute of Allergy and Infectious Diseases. Dengue Fever. Baltimore, MD: National Institutes of Health, 2005.

6. Rico-Hesse, Rebecca. Dengue Virus Evolution and Virulence Models. Clinical Infectious Diseases 2007; 44: 1462-5.

7. Vasilakis N, Cardosa J, Hanley KA, et al. Fever from the forest: prospects for the continued emergence of sylvatic dengue virus and its impact on public health. Nat Rev Microbiol 2012; 9(7): 532—541.

8. Tsai J-J T, et al. The Importance of Hematopoeitic Progenitor cells in Dengue. Therapeutic Advances in Hematology 2011; 3(1): 59-71. Kuhn R, Zhang W, Rossmann WG, et al. Structure of Dengue Virus: Implication for Flavivirus Organization, Maturation, and Fusion. Cell 2002; 108: 717-725.

9. Hammond SN, et al. Difference in Dengue Severity in Infants, Children, and Adults in a 3-year Hospital Based Study in Nicaragua. Am J of Tropical Medincine Hyg 2005; 73: 1063-70.

10. Pooja C, Amrita Y, and Viney C. Clinical Implication and Treatment of Dengue. Asian Pacific Journal of Tropical Medicine, 2014: 169-178.

11. Noisakran S and Perng GC. Alternate Hypothesis on the Pathogenesis of Dengue Hemorrhagic Fever (DHF/Dengue Shock Syndrome (DSS) in Dengue virus Infection. Exp Biol Med 2008: 3(4): 401-8.

12. Martina BE, Koraka P, and Osterhaus ADME. Dengue Virus Pathogenesis: An Integrated View. Clinical Microbiology Review 2009; 22 (4): 564-581.

13. Sun P, Bauza K, Pal S, et al. Infection and Activation of Human Peripheral Blood Monocytes by Dengue viruses through the Mechanism of Antibody-Dependent Enhancement. Virology 2011; 421: 245 —252.

14. Domingues RB, Kuster GW, Onuki-Castro FL, et al. Involvement of the Central Nervous System in Patients with Dengue Virus Infection. Journal of Neurological Sciences 2008; 267: 36-40.

15. Solomon T, Dung NM, Vaugh DW, et al. Neurological Manifestations of Dengue Infection. Lancet 2000; 355: 1053-59.

16. Carod-Artal FJ, Farrar WJ, and Gascon J. Neurological Complications of Dengue Virus Infection. Lancet Neurol 2013; 12: 906-19.

17. Puccioni-Sohler M and Orsini M. Dengue: A New Challenge for Neurology. Neurology International 2012; 4e15: 65-70.

18. Verma R, Sharma P, Garg RK, et al. Neurological Complications of Dengue Fever: Experience from a Tertiary Center of North India. Ann Indian Academy of Neurol 2011; 14(4): 272-278.

19. Salgado DM, et al. Heart and Skeletal Muscle are Targets of Dengue Infection. Pediatr Infect Dis J 2010; 29(3): 238—242.

20. Yacoub S, et al. Cardiovascular Manifestations of the Emerging Dengue Pandemic. Nat Rev Cardiol 2014.

21. Soek-Siam T and Mohamad AB. The clinical features and outcomes of acute liver failure associated with dengue infection in adults: a case series. Brazilian J of Infectious Diseases 2013; 17(2): 164—169.

22. Gulati S and Maheshwari A. Atypical Mani-

festations of Dengue. Tropical Medicine and International Health 2007; 12(7): 1087-1096.

23. Brij M, Patwari AK, and Anand VK, Hepatic Dysfunction in Childhood Dengue Infection. J of Trop Pediatr 2000; 46: 40-45.

24. Setiawan MW, Samsi TK, Wulur H, et al. Dengue Hemorrhagic Fever: Ultrasound as an aid to predict severity of the disease. Pediatr Radiol 1998; 28: 1-4.

25. Reddy KRB, Ramesh R, Veerappa, and Shivananda. Ultrasonography as a tool in predicting the severity of dengue in children- a useful aid in developing country. Pediatr Radiol 2013; 43: 971

26. Cheepsattayakorn A and Cheepsattayakorn R. Dengue Virus Infection: Lung Involvement, Clinical Implications, and Associated Human Leukocyte Antigens. J of Repiratory Medicine Research and Treatment. 2014; 14 pages. ID 162245.

27. Wang, CC, et al. Chest Radiographic Presentations in Patients with Dengue Hemorrhagic Fever. Am J Trop Med Hyg 2007; 77 (2): 291-96.

28. Rodrigues RS, et al. Lung in Dengue: Computed Tomography Findings. PLoS ONE. 2014; 9(5): e96313.

29. Koshy J and Pandian JD. Dengue Infection: An Emerging Cause of Neuromuscular Weakness. J of Neurosci Rural Pract 2012; 3 (1):1-4.

30. Koshy J, John M, Rathore S, and George UB. Spontaneous Muscle Hematoma in a Patient with Dengue Hemorrhagic Fever. CHRISMED J 2014; 1: 201-202.

31. Garg RK, Malhotra HS, and Malhotra KP. Dengue-Associated Neuromuscular Complications 2015; 63: 497-516.

Corresponding Author:

Mariaem M. Andres, MD
St. Luke's Medical Center, Philippines
Email: mariaem139@yahoo.com

Multimodality Imaging in the Evaluation of Parasitic Twinning

Scott Riley K. Ong, MD; Alvin C. Camacho, MD; Romelito Jose G. Galsim, MD; Renato M. Carlos, MD; and Gerardo L. Beltran, MD*

Department of Radiology, Philippine General Hospital

Abstract

Parasitic twinning is an extremely rare anomaly that is estimated to occur once in every 1 to 2 million live births. It represents an asymmetric form of conjoined twins, wherein one twin fails to undergo normal development in utero and becomes vestigial and completely dependent on the other. Because of its rarity and potentially complex anatomic issues, its management may be challenging especially for surgeons. Imaging plays an important role, especially for pre-operative planning. A case of parasitic twins, presenting with supernumerary limbs and other truncal and cranial anomalies, is hereby reported. Multimodality imaging workup, comprising of computed tomography, magnetic resonance imaging, contrast enema and angiographic studies, was performed. Its results are presented and discussed, emphasizing the structural details and anatomic issues posed by the patient and her parasitic twin.

Introduction

Conjoined twins are a rare phenomenon that occurs during monochorionic-monoamniotic twin gestation when the embryo divides at 13 to 15 days after conception and the resulting pair does not fully separate.[1] It is estimated to occur once in every 50,000 to 100,000 births. [2]

Conjoined twins may be classified as either symmetric or asymmetric, depending on the extent of development of each embryo. The latter case, which is also known as parasitic or heteropagus twinning, occurs when one of the twins fails to undergo normal development during gestation and becomes vestigial and dependent on the other. [2,3] The exact pathogenesis for such an event remains uncertain, but is possibly due to an ischemic event in utero that results in the death of one of the twins. [3,4] The underdeveloped, typically smaller twin is referred to as the parasite, while the normal, fully developed host is referred to as the autosite. This form of twinning is exceedingly rare, accounting for only 10% of conjoined twins, and is estimated to occur once in every 1 to 2 million live births. [3]

A rare case of parasitic twinning is hereby reported. Comprehensive radiologic workup—consisting of whole body CT scan, pelvic CT angiography, craniospinal MRI, four-vessel cerebral angiography, and contrast enema—was performed to evaluate the patient's anatomy.

Clinical Presentation

A 2-year old female was admitted to the Philippine General Hospital (PGH) on December 2014 for surgical management of parasitic twinning. She was born full-term to a then 29-year old, primiparous mother. Obstetric sonography done at 3 and 6 months age of gestation revealed the presence of four lower extremities and an abnormal protuberance in the occiput of the fetus. The course of the pregnancy was otherwise unremarkable. A strong history of twinning, both fraternal and identical, was noted in both maternal and paternal sides of the family.

Due to the presence of supernumerary limbs,

elective cesarean delivery was performed. Upon birth, the patient had a good cry and good activity with no sensorial changes or seizure episodes. However, cranial CT scan done on her second day of life revealed hydrocephalus with colpocephaly and an occipital encephalocele. Ventriculoperitoneal shunt insertion was performed. She was eventually discharged in good condition and advised to undergo surgical repair which was deferred due to financial constraints.

Upon admission to PGH, physical examination showed the presence of supernumerary lower limbs, as well as anomalies in the patient's head and back. Four lower extremities, arbitrarily designated as limbs A to D, were noted (Figure 1). Grossly, the pair of limbs B and C appeared to be the lower extremities of the autosite while the pair of limbs A and D appeared to be the lower extremities of the parasite. Limbs B and C exhibited normal motor strength (grade of 5/5) and intact sensation (100%). Limb A showed decreased motor strength (grade of 3/5) but intact sensation (100%), while limb D demonstrated both poor motor strength (grade of 1/5) and poor response to sensory stimuli (25%).

Examination of the patient's head and back showed a prominent occipital protuberance. An accessory soft tubular structure was noted to arise from the occiput and extend to her lower back (Figure 1). At the region where this structure inserted into her lower back, two short anomalous limbs were seen. These appeared to represent the underdeveloped upper extremities of the parasite and had no sensorimotor function. The remainder of the physical examination was unremarkable.

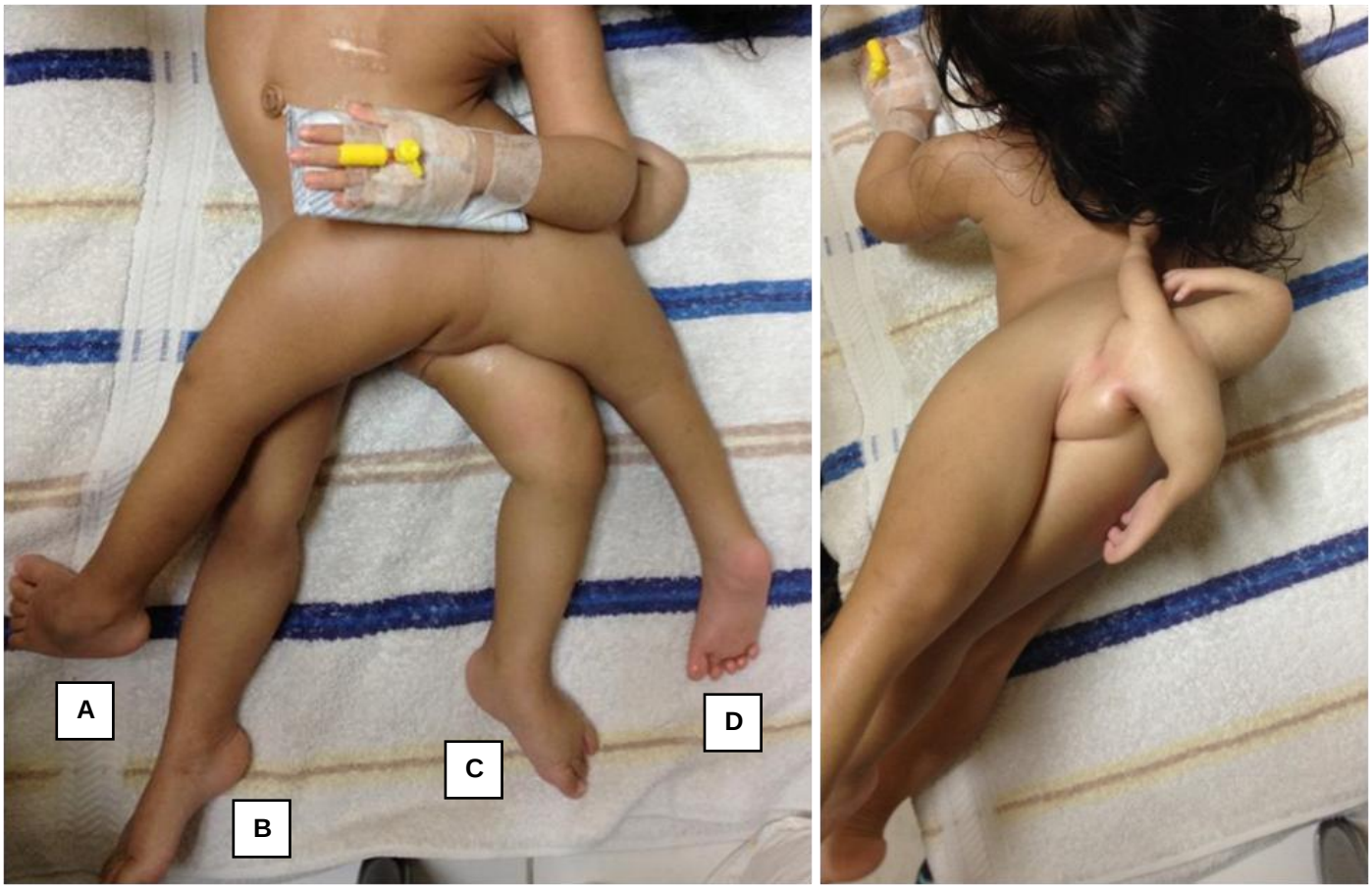

Figure 1. Photographs of the patient in anterior (left) and posterior (right) views showing four lower extremities, an accessory tubular structure (arrow) along her back, and anomalous short upper extremities arising from her lower back.

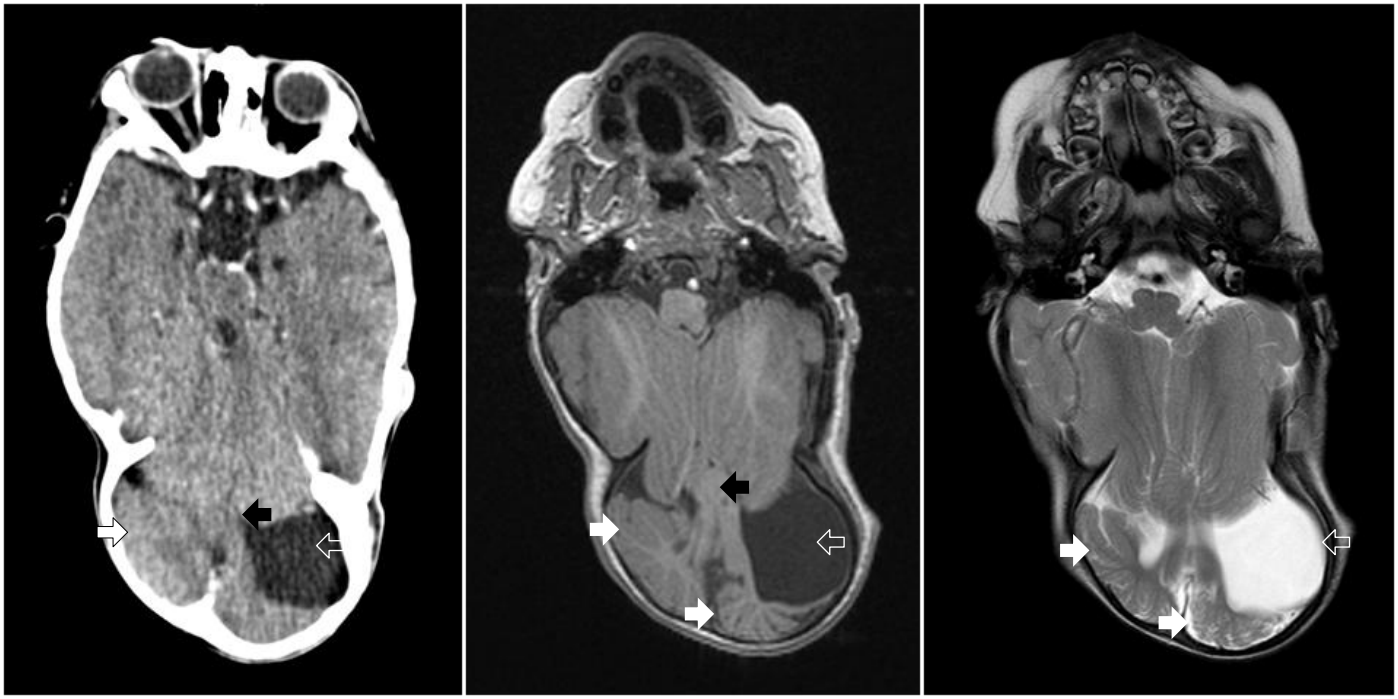

Figure 2. Axial CT (left), T1-weighted (middle) and T2-weighted (left) images showing a defect on the occipital bone and the parasite's dysmorphic cranium posterior to it. Cerebellar structures (white arrow), a rudimentary brainstem (black arrow), and a cystic extraaxial focus (open arrow) were seen within it.

Radiologic Findings

The patient had a dolichocephalic skull with premature fusion of the sagittal suture. The cerebral hemispheres appeared mildly dysmorphic, with a portion of the right mesial occipital lobe seen crossing the midline. Callosal dysgenesis was observed, with an underdeveloped splenium and a relatively well-developed rostrum.

A defect was noted in the occipital bone. Posterior to this was what appeared to be the dysmorphic cranium of the parasite. Parts of the autosite's occipital lobe and cerebellum were seen partially herniating through the said defect into the dysmorphic cranium. Cerebellar structures and a rudimentary brainstem, presumably those of the parasite, were also seen within it. Additionally, a cystic extraaxial focus, likely representing an arachnoid cyst, was seen within its left aspect (Figure 2).

Angiography demonstrated the major vascular supply of the parasite's dysplastic brain to arise from the autosite's left posterior inferior cerebellar artery and superior cerebellar arteries (Figure 3). Venous drainage occurred via the autosite's torcular herophili.

Within the subcutaneous layer of the posterior cervical region, a loculated soft tissue mass with

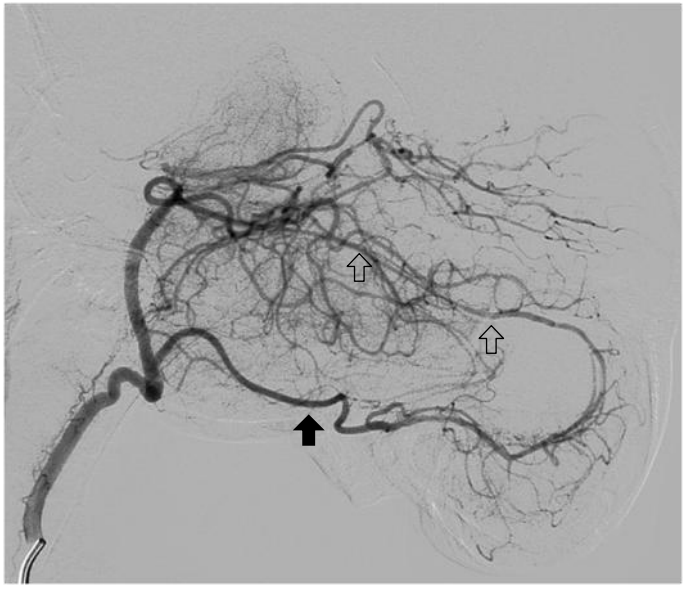

Figure 3. Left vertebral angiogram demonstrating the vascular supply of the parasite's dysplastic brain (bracket) arising from the left posterior inferior cerebellar artery (solid arrow) and superior cerebellar arteries (open arrow).

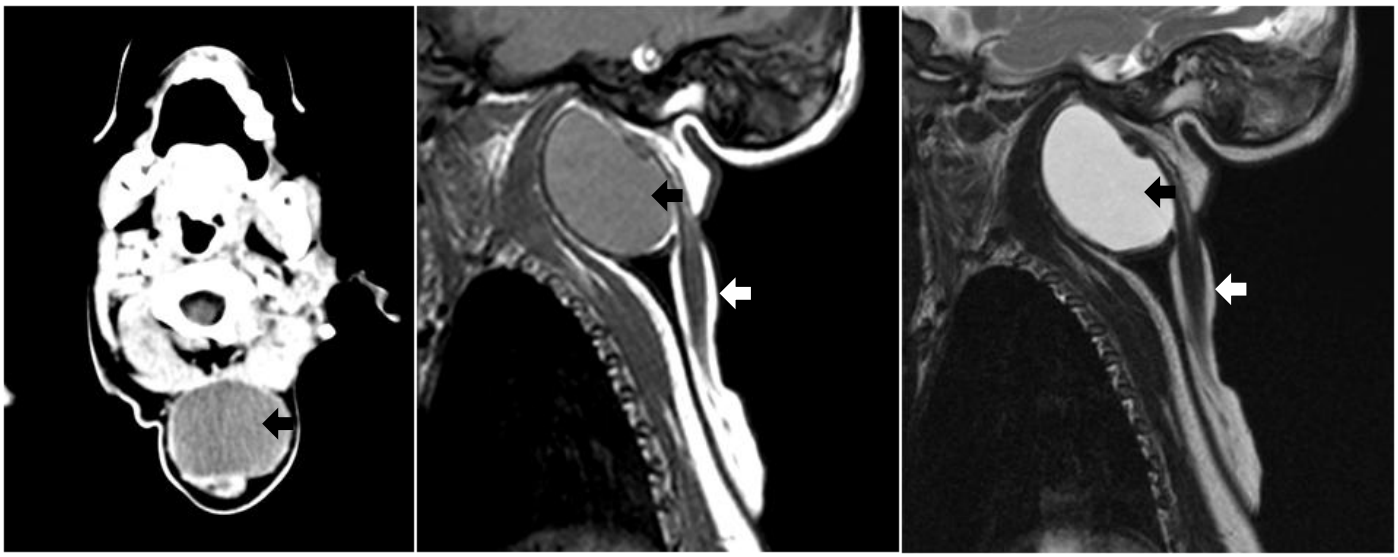

Figure 4. Axial contrast-enhanced CT (right), sagittal T1-weighted (middle) and sagittal T2-weighted images showing a soft tissue mass in the posterior cervical region (black arrow) and an accessory tubular structure arising from the autosite's occiput and coursing inferoposteriorly (white arrow).

minimal peripheral enhancement was noted. There was no communication between it and the spinal canal. MRI signal patterns were suggestive of a dermoid cyst. From the said mass, the clinically apparent accessory tubular structure was seen coursing inferoposteriorly to the autosite's lower back. It exhibited a soft tissue core surrounded by subcutaneous tissues and skin and most likely represents the parasite's vestigial truncal tissue (Figure 4).

Spinal dysraphism and tethered cord were present with fusion and segmentation anomalies from the level of the L4 vertebra to the sacrum. Dorsal fusion defects were seen in the sacrum, through which fat and neural elements herniated as a lipomyelomeningocele.

Vestigial sacral structures fused with the posterior elements of the autosite's sacrum were identified. Articulating with these was the dysmorphic pelvic of the parasite. CT imaging revealed that limbs C and D arose from the dysmorphic pelvis while limbs A and B articulated with the autosite's pelvis (Figure 5). In contrast to the gross morphologic appearance of the patient's lower extremities, limbs A and B appeared to represent the autosite's left and right lower extremities, respectively, while limbs C and D represented those of the parasite.

CT angiography showed that limbs A and B were supplied by the autosite's left and right external iliac arteries, respectively. The left internal iliac artery was increased in caliber relative to the right and gave rise to a prominent, anomalous branch to the parasite's dysmorphic pelvis. Two major braches from this continued as

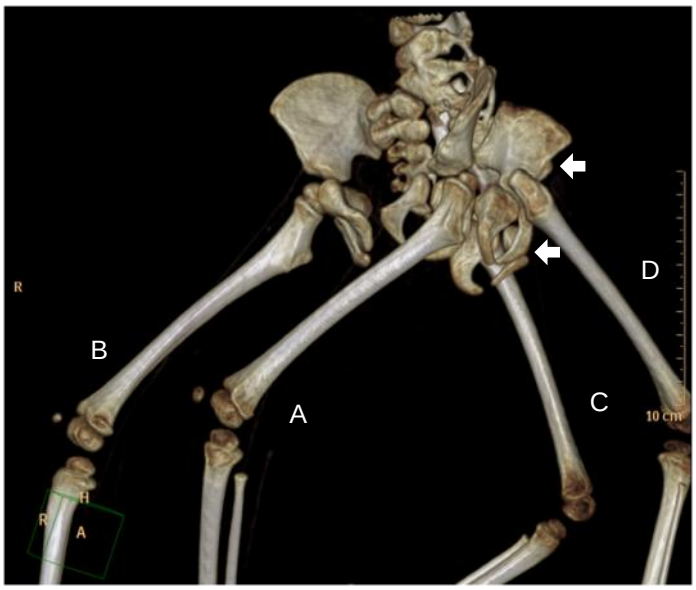

Figure 5. CT reconstruction demonstrating the skeletal framework of the patient's pelvic girdle, with limbs A and B arising from the autosite's pelvis and limbs C and D arising from the parasite's dysmorphic pelvis.

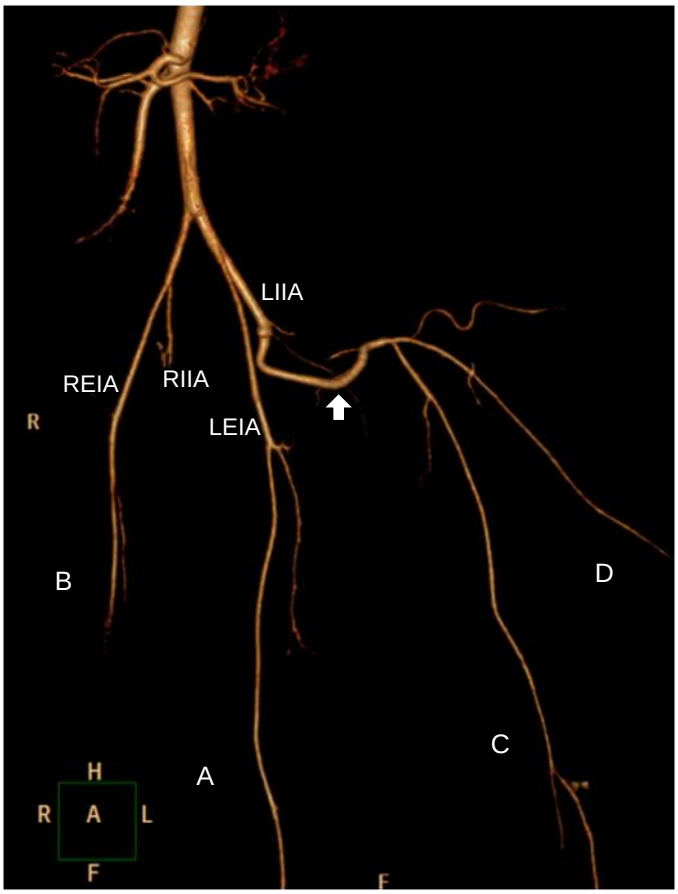

Figure 6. CT angiogram demonstrating the arterial framework of the patient's pelvis and lower extremities. [Right external iliac artery (REIA), right internal iliac artery (RIIA), left external iliac artery (LEIA), left internal iliac artery (LIIA), anomalous branch to the parasite's dysmorphic pelvis (arrow)]

the vascular supplies of limbs C and D (Figure 6).

Elongated, tubular structures resembling rudimentary bowel loops were seen within the parasite's dysmorphic pelvis, posterior to the autosite's rectum. Intraluminal hyperdensities, which may represent secretions or calcifications, were noted. However, contrast enema showed no communication between these structures and the autosite's bowels (Figure 7).

Figure 7. Axial CT images (right) showing tubular structures resembling rudimentary bowel loops within the parasite's pelvis, and contrast enema (left) demonstrating no communication between these and the autosite's bowels.

Discussion

A parasitic twin most commonly presents as supernumerary limbs externally attached to the autosite. It is not uncommon for it to contain some viscera, but it very rarely presents with a functional heart or brain. Among the eight types of conjoined twinning in Spencer's classification, four typically present with supernumerary lower limbs—namely, rachipagus, parapagus, ischiopagus, and pygopagus.[5]

In the current case, the presence of supernumerary lower limbs apparently arising from the patient's pelvis served as the dominant anatomic feature of the parasite. Based on clinical examination alone, the exact point of attachment of these structures to the autosite could not be ascertained. Identifying which among these represented those of the parasite and which were those of the autosite could not be made with confidence. However, with the use of imaging, it was demonstrated that limbs C and D represented the lower extremities of the parasite and they were attached to the dorsal aspect of the autosite's sacrum by means of a dysmorphic pelvis and vestigial sacrum. Other than the noted fusion and segmentation anomalies from the L4 vertebra to the sacrum, where the parasite's lower extremities established their connection, the remainder of the patient's vertebrae were unremarkable. These findings support the diagnosis of parasitic pygopagus.

A remarkable aspect of this case is the presence of other vestigial structures from the parasite in addition to its lower limbs. A dysmorphic cranium with a rudimentary brainstem and relatively developed cerebellum was identified posterior to the autosite's occiput. Angiography clearly demonstrated the dependence of the parasite's brain on the autosite's vertebrobasilar circulation for blood supply. A tubular structure that may represent vestigial truncal tissue and a pair of rudimentary upper limbs were also noted at the patient's back.

Parasitic twinning is an extremely rare event and its management may pose unique surgical challenges. Multimodality imaging permitted detailed elucidation of the patient's anatomy and was indispensable for pre-surgical planning. The presence of additional anomalies, such as callosal dysgenesis, arachnoid and dermoid cysts, lipomyelomeningocele and tethered cord, which otherwise cannot be detected through clinical examination alone, were also diagnosed.

Ethical Considerations

Informed consent allowing the investigators to review the patient's health information and publish her case was obtained from her parents. The patient's identity and right to privacy were respected. The use of her depersonalized photographs was done with permission.

This case report has been registered at the University of the Philippines Manila Research Ethics Board.

References

1. 1. Egan JFX, Borgida AF. Ultrasound Evaluation of Multiple Pregnancies. In: Callen PW, editor. Ultrasonography in Obstetric and Gynecology. 5th ed. Philadelphia, PA: Saunders Elsevier, PA; 2007: 279-80.

2. 2. Hwang EH, Han SJ, Lee JS, Lee MK. Unusual Case of Monozygotic Epigastric Heteropagus Twinning. J Pediatr Surg 1996; 31 (10): 1457-60.

3. 3. Sahu, SJ, Choudhury PR, Gogoi J, Das TK, Talukdar KL, Bayan H. Heteropagus

Parasitic Conjoined Twin — A Case Report. Int J Health Sci Res 2015; 5(3): 383-87.

4. 4. Satter E, Tomita S. A case report of an omphalopagus heteropagus (parasitic) twin. J Pediatr Surg 2008; 43: E37-E39.

5. 5. Corona-Rivera JR, Corona-Rivera E, Franco-Topete R, Acosta-León J, Aguila-Dueñas V, Corona-Rivera A. Atypical Parasitic Ischiopagus Conjoined Twins. J Pediatr Surg 2003; 38(2): E3.

Corresponding author:
Scott Riley K. Ong
70-D Simoun St., Sto. Domingo
Quezon City, Philippines 1100
Phone: (632)7415359
scottrileyong@yahoo.com

"Sweet Potato Leg" : A Case Report on the Importance of Medical Imaging in the Diagnosis of Klippel-Trenaunay Syndrome

James II G. Casuga, Susan R. Gaspar-Mateo, Samuel B. Bangoy, Maria Theresa T. Sanchez, Derly R. Principe-Valderrama
Southern Philippines Medical Center, Davao City, Philippines

Abstract

Klippel-Trenaunay Syndrome (KTS) is a complex-combined vascular malformation presenting as capillary venous lymphatic malformations with overgrowth. (1) The exact cause of this syndrome remains unclear, although various theories have been proposed. This syndrome is characterized by a triad of capillary malformations, atypical varicosities or venous malformations and bony or soft tissue hypertrophy, and usually affects one extremity. Its incidence is sporadic without gender or racial predilection. We report a 5 year-old girl suffering from KTS, originated from Kidapawan City, Philippines, whose diagnosis and successful management relied on concerted effort by multidisciplinary team approach.

Introduction

Klippel-Trenaunay Syndrome (KTS), a rare complex disease with a prevalence of about 1:100,000 population [2], is classified as a complex-combined vascular malformation presenting as capillary venous lymphatic malformation with overgrowth. [1] As cited by De leon, et al, [3] these venous abnormalities are thought to be caused by deep venous obstruction or deep venous atresia. The diagnosis and successful treatment of such case frequently require a multidisciplinary effort. [1] Although KTS is often a progressive disorder, and complications may be life-threatening, many individuals can survive with their symptoms. [4] Early detection and intervention can help to optimize the life quality of affected patients.

The objectives of this case report are: a) to discuss a case of Klippel-Trenaunay Syndrome; b) to review the differential diagnosis, epidemiology, clinical presentation, pathology, as well as complications and c) to illustrate the role of radiological and imaging studies in the diagnosis and management of the syndrome.

Case Report

A 5-year old, female Filipino, presented with progressively enlarging right lower extremity with cutaneous scabbing, bleeding and recurrent infection. The history dated back to birth when she was born with a diffuse patchy erythematous lesion in the right lower limb, shortly extending to the thigh, leg and foot with progressive spread to the right lower extremity up to the buttocks, groin and pudendal areas. Insidious bleeding, cutaneous scabbing (with verrucous hyperpigmented plaques developed over the lesion) and infections interspersed with periods of improvement were noted. These circumstances caused repetitive admissions to a tertiary private hospital for temporizing bleeding control and antibiotic treatment for cutaneous infections. She was treated with steroids and alpha interferon trials on maximal doses, propranolol and vincristine but the lesions and symptoms were not alleviated but continuously progressed. The patient had no family history of the disorder. The rest of the past medical, growth and development, personal and social histories were unremarkable

No conclusive diagnosis has ever been made. A multidisciplinary team initially managed this case as extensive lower extremity congenital hemangioma.

Physical Examinations

Physical examinations revealed abnormalities in the right lower extremity, bilateral buttocks, and groin and pudendal areas. The overlying erythematous, plaque laden and scabbed warm skin and the underlying soft tissues were thick, especially in both gluteal regions down to the entire right lower limb. Areas with various ages of clots, scabbing and verrucous hyperpigmented plaques were demonstrated more in the leg and foot (Figure 1). Bruits were not appreciated. The rest of the physical examinations was unremarkable.

Laboratory results on complete blood count (CBC) were within normal limits with no evidence of infection. X-ray of the lower limb showed heterogeneous soft tissue densities related to the crusted lesions. There was associated increased bone density in the right tibia and fibula.

Magnetic Resonance Imaging (MRI) (Figure 2) revealed diffuse enlargement of right lower extremity with thickening/hypertrophy of the soft tissue involving the skin and subcutaneous layers of the visualized gluteal and perineal regions bilaterally, as well as the right upper thigh down to the foot. Diffuse and scattered flow voids (some are dilated); as well as serpiginous structures with nonspecific pattern are seen within the thickened soft tissues. T2WI revealed dilated tubular structures with high signal intensity (which are characterized as flow void on T1WI) notably seen within the subcutaneous and intramuscular areas of the thigh and leg. MRI features are suggestive of diffuse soft tissue hypertrophy with mixed vascular malformations in the right lower limb.

Conventional angiography (Figure 3) showed multifocal capillary and venous malformations characterized by fine twigs or "puff of smoke" appearance and early opacification of draining veins was noted in the right lower extremity

Figure 1. This image depicts that the right lower extremity is enlarged compared with the normal left side. (*Inset*) Magnified Plantar view shows multiple varisized verrucous hyperpigmented plaques and scabbing (*arrow*) on the erythematous right foot.

Figure 2. Magnetic Resonance Imaging in T1WI (coronal view). (A) non-contrast and (B) contrast —enhanced T1W MRI images of the patient showing diffuse soft tissue hypertrophy with mixed vascular malformations in the right lower limb (*arrow*), exhibiting multiple scattered intramuscular and subcutaneous flow voids with variable enhancement patterns.

with delayed contrast wash-out in venous phase. Multiple feeding vessels arising from the superficial femoral artery, tibioperoneal, anterior and posterior tibia and plantar arteries were also noted. Thus, features of conventional angiogram were suggestive of multifocal capillary and venous malformations.

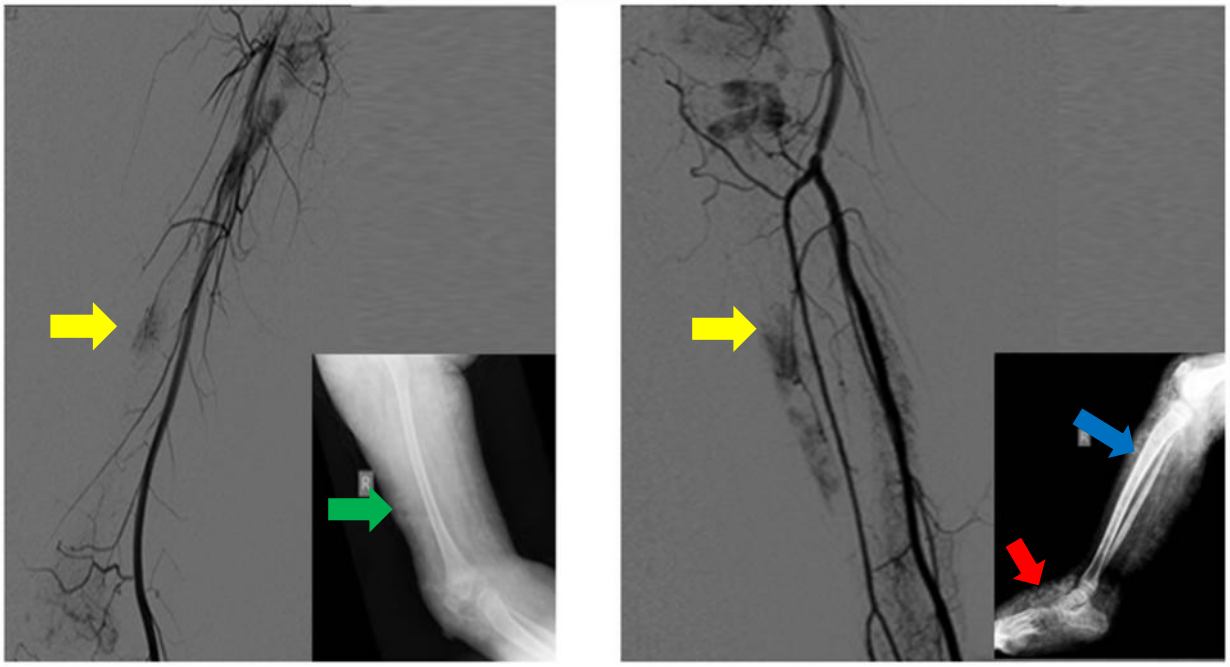

Figure 3. Conventional angiogram of the right thigh. (A-thigh, B-leg) There are multifocal capillary and venous malformations (yellow arrows). (Inset- corresponding lateral view radiographs)(A) Soft tissue swelling of the thigh (green arrow) and heterogeneous densities over soft tissue of the foot relating to underlying crusted lesions (red arrow). Increased cortical bone density is also present right tibia and fibula (blue arrow).

Differential Diagnoses

VASCULAR TUMORS [1]
Hemangioma
- Infantile hemangioma
- Congenital hemangioma
- Rapidly involuting congenital hemangioma (RICH)
- Noninvoluting congenital hemangioma (NICH)
- Kaposiform hemangioendothelioma

VASCULAR MALFORMATIONS [1]
Simple Slow-flow
- Venous malformation (VM)
- Lymphatic malformation (LM)
- Capillary malformation (CM)

Simple Fast-flow
- Arteriovenous malformation (AVM)
- Arteriovenous fistula (AVF)

Complex-combined Slow-flow
- Klippel-Trenaunay syndrome: capillary venous lymphatic malformation (CVLM) with overgrowth.

Complex-combined Fast-flow
- Parkes Weber syndrome: capillary arterial venous malformation (CAVM) with overgrowth

Table 1. Differential Diagnoses of Our Case

The patient presented with a congenital skin lesion, which progressively grew out of proportion with her age. Patient was neither responsive to interferon, prednisone, propanolol nor vincristine, which made hemangioma less likely. Proteus syndrome was considered but later excluded due to the disease's hallmark feature of random or mosaic distribution of multifocal overgrowth of tissue throughout the body, which was not the feature of this case. [3] Parkes Weber Syndrome (PWS) can have features of limb overgrowth and congenital capillary malformations [5] but usually includes multiple small arteriovenous malformations or shunts within a capillary arteriovenous lesion. The above lesion was not present in our patient. Physical examinations and imaging findings of: a) diffuse erythematous lesions in the entire right lower limb with verrocous hyperpigmented plaques of various sizes, b) diffuse soft tissue hypertrophy with mixed vascular malformations and c) diffuse multifocal capillary and vascular malformations correlate best with the triad of Klippel-Trenaunay syndrome.

Discussion

Klippel-Trenaunay Syndrome, initially described in 1900, is a triad of cutaneous capillary hemangiomas, bony and soft tissue hypertrophy, and venous dilations, a disorder usually affects only a segment of the body with varied clinical manifestations as was seen in our patient. [6] This rare congenital malformation, [7] was originally known as Klippel-Trenaunay Weber Syndrome. However, to avoid confusion with Parkes Weber Syndrome, "Weber" was dropped. [8] Most cases of KTS are sporadic and there is no recognized gender or racial predilection. [2] The prevalence of KTS is about 1:100,000. [9]

Tortuous varicose veins are present at birth as in this case. They usually become more prominent at a later stage and progress until adolescence. [10] These veins usually begin at the foot or leg, and grow progressively to involve the buttock or gluteal region. These areas may remain stable or enlarge gradually, causing pain, lymphedema, thrombophlebitis, and ulcers. [11] Hypertrophy is the third symptom to appear in the syndrome and it can be secondary to length increase (bone involvement) and/or circumference increase (soft tissue involvement). It can be observed at birth and progresses during the first year of life. The above temporal changes have been systematically and consistently observed in our patient. In adolescence, when the child's growth cycle period has finished, the limb will

stop growing. [3] The above explains the decision of the multidisciplinary to adopt a conservative approach for this child.

The exact cause of Klippel-Trenaunay-Weber syndrome (KTWS) remains to be elucidated, although several theories exist including intrauterine damage to the sympathetic ganglia or intermediolateral tract leading to dilated microscopic arteriovenous anastomoses [5] or deep vein abnormalities, with resultant venous flow obstruction of venous flow, development of varices, and limb hypertrophy. [12] Other theories include mesodermal defect or mixed mesodermal and ectodermal dysplasia responsible for the development of KTWS. [13-14], Lastly, it may result from a pathogenic gene for vascular and tissue overgrowth. [9]

Bleeding and cellulitis (infection of the skin) and pain are common complications of KTS. [8] Gastro-intestinal or genitourinary hemorrhage occurs if there is visceral involvement. [9] If capillary malformations are large enough, they may sequester platelets, possibly leading to the Kasabach-Merritt syndrome (consumptive coagulopathy). [9]

There is no cure for this disorder. [3] Therapy aims to improve the patient's condition and treat the consequences of severe lesions and length discrepancy. Port-wine stains are usually treated with pulsed dye laser therapy. [6, 8] Varicose veins are managed by the use of compression stockings to address venous insufficiency, swelling and pain. Sclerosing therapy, injecting a chemical agent into the vein is used to destroy veins in some patients. [11] Surgical treatment is only reserved in symptomatic cases of superficial varicose veins. [8]

Conclusion

Klippel-Trenaunay syndrome is diagnosed and followed up with combination of clinical, laboratory and imaging tools including radiographs, MRI and conventional angiography. This syndrome is rare, complex, progressive, whose complications may be life-threatening. However, the quality of life of the affected patients can be optimized by efficient infection and bleeding control. Correct diagnosis depends on the synergic multidisciplinary approach by understanding the characteristic imaging features and classical temporal disease process.

References

1. Caffey's Pediatric Diagnostic Imaging 11th edition by Thomas L. Slovis. 2008
2. Esterly NB. Haemangiomas. In: Harper J, Oranje A, Prose N, eds. Textbook of pediatric dermatology. Oxford: Blackwell Science, 2000:997-1016.
3. Cristiano do Amaral de Leon, et. Al. Anais Brasileiros de Dermatologia. vol.85 no.1 Rio de Janeiro Jan./Feb. 2010 http://dx.doi.org/10.1590/S0365-05962010000100015
4. Eberhard DA. Two-year-old boy with Proteus syndrome and fatal pulmonary thromboembolism. Pediatr Pathol 1994; 14:771—779./ RadioGraphics 2004; 24:1051—1068 . Published online 10.1148/rg.244035726
5. Bliznak J, Staple TW. Radiology of angiodysplasias of the limb. Radiology. Jan 1974;110(1):35-44.[Medline]Baskerville PA, Ackroyd JS, Browse NL. The etiology of the Klippel-Trenaunay syndrome. Ann Surg. Nov 1985;202(5):624-7

6. Kotze PG, Soares AV, Lima MC, Balidn-Junior A, Sartor MA, Bonardi RA. Síndrome de Klippel-Trenaunay: Uma causa rara de hemorragia digestiva baixa. Rev Bras Coloproct. 2002; 22:109-112.

7. Jacob AG et al (1998) Klippel-trennaunay Syndrome: Spectrum and Management. Mayo clin proc 73:28-36

8. http://www.sturge-weber.org/medical-matters/klippel-trenaunay-syndrome.html

9. Kihiczak GG, Meine JG, Schwartz RA, Janniger CK. Klippel-Trenaunay syndrome: a multisystem disorder possibly resulting from a pathogenic gene for vascular and tissue overgrowth. Int J Dermatol. Aug 2006;45 (8):883-90. [Medline]. / Cha SH, Romeo MA, Neutze JA. Visceral manifestations of Klippel-Trénaunay syndrome. Radiographics. 25 (6): 1694-7. doi:10.1148/rg.256055042 - Pubmed citation / Copel J. Obstetric Imaging. Elsevier Health Sciences. (2012) ISBN:1437725562.

10. Garzon MC, Huang JT, Enjolras O, Frieden IJ. Vascular Malformations/Part II: Associated syndromes. J Am Acad Dermatol. 2007;56:541-64.

11. Tonsgard JH, Fasullo M, Windle ML, McGovern M, Petry PD, Buehler B. Klippel-Trenaunay-Weber Syndrome. Pediatrics: General Medicine Articles 2006. [acesso 16 Ago. 2008]. Disponível em: http://www.emedicine.com/derm/topic213.htm

12. Servelle M. Klippel and Trenaunay's syndrome. 768 operated cases. Ann Surg. Mar 1985;201(3):365-73

13. Baskerville PA, Ackroyd JS, Browse NL. The etiology of the Klippel-Trenaunay syndrome. Ann Surg. Nov 1985;202(5):624-7. [Medline].

14. McGrory BJ, Amadio PC. Klippel-Trenaunay syndrome: orthopaedic considerations. Orthop Rev. Jan 1993;22(1):41-50. [Medline].

Disclosure: This case was presented before SPMC-SPH Teaching Files Monthly Conferences and presented at the Philippine College of Radiology- Southern Mindanao Chapter Annual Case Presentation Contest.

Surfer's Myelopathy in an Adolescent Male

Hannah Regina G. Villalobos,[1] Mariaem M. Andres,[1,2] Bernard F. Laya,[1,2]

[1] St. Luke's Medical Center-Quezon City, Philippines
[2] St. Luke's Medical Center-Global City, Philippines

Abstract

Surfer's myelopathy is a rare spinal cord injury with few reported cases. The etiology is poorly understood but believed to be due to a vascular phenomenon from repetitive hyperlodotic posturing while surfing. Recent studies reveal that it has typical magnetic resonance imaging (MRI) appearance. Most reported cases had been in adults and there is paucity of publications in the pediatric population. We report a case of a15-year-old male with a history, clinical course, and imaging manifestations typical for surfer's myelopathy.

Introduction

Surfer's myelopathy is an acute non-traumatic myelopathy typically affecting the thoracolumbar spine [1]. The overall incidence is unknown. The largest case series of 23 patients was reported by Nakamoto and colleagues in Hawaii. The common presentation was of novice surfers with prolonged hyperlordosis (hyperextension) of the spine on a surfboard who later developed back pain, which progressed to paraesthesia and lower extremity weakness. These patients were all previously healthy, and other than the act of surfing, there was no recent traumatic event. Most of the reported cases are in adults and there is paucity of literature on surfer's myelopathy the pediatric age group. This is a case report of a 15-year-old male with a history and clinical manifestations of surfer's myelopathy, demonstrating the typical MRI features upon presentation.

Case Report

A previously healthy, 15-year-old male took surfing class for the first time. An hour after surfing, he began to feel mild low back pain that progressed to severe pain within an hour. Paraesthesia of both lower extremities developed, which eventually progressed to paralysis of both lower extremities, along with urinary incontinence. Within 22 hours, he was brought to a tertiary medical center for management. Upon hospital presentation, his vital signs were stable and his respiratory, cardiovascular, and abdominal examinations were normal. Mental status, speech, cerebellar and cranial nerve examinations were also normal. His neck was soft without rigidity. Sensory examination showed decreased sensation in the lower extremities with an approximate range of 50 -75%. He later lost his ability to stand and walk with 0/5 strength of the lower extremities. The Babinski response was absent bilaterally. The rectal examination showed absent sensation and decreased sphincter tone. He had no previous surgery, no history of recent trauma, and no flu-like symptoms in the preceding weeks prior to presentation. Laboratory tests were unremarkable, except for a mild leukocytosis with a neutrophilic predominance.

Thoracic and lumbosacral spine radiographs were unremarkable. A day after admission, MRI of the thoracic and lumbar spine revealed centromedullary T2 weighted (T2W) and short tau

inversion recovery (STIR) abnormal hyperintense signals in the spinal cord from T8 to the conus medullaris. There was associated cord expansion but no distinct abnormal contrast enhancement was seen [Fig. 1]. These findings are most consistent with spinal cord oedema. From the clinical and imaging manifestations, he was diagnosed to have Surfer's myelopathy. A course of steroids was given along with antibiotics, proton pump inhibitors, vitamin B complex, and a neurotrophic agent for 9 days. He also underwent physical therapy during the hospital stay. The sensation over his lower extremities improved to 80-90%, along with improved motor strength, and he was discharged after 18 days. A repeat MRI of the thoracic and lumbosacral spine was obtained four months after his initial presentation, which showed significant regression of the cord expansion and abnormal hyperintense T2W signals [Fig. 2].

Discussion

Surfer's myelopathy was first described in 2004 as an acute non-traumatic spinal cord injury, occurring most commonly in novice surfers [2]. Although no definite histopathological confirmation has been published, surfer's myelopathy probably results from a vascular pheno-

Figure 1. Sagittal MRI of the thoracolumbar spine at day 2 of hospitalization. Sagittal T2W image (A) reveals an expanded spinal cord from T8 to conus medullaris with abnormal increase signal representing cord edema. Sagittal T1 image following intravenous administration of gadolinium (B) demonstrate no abnormal contrast enhancement.

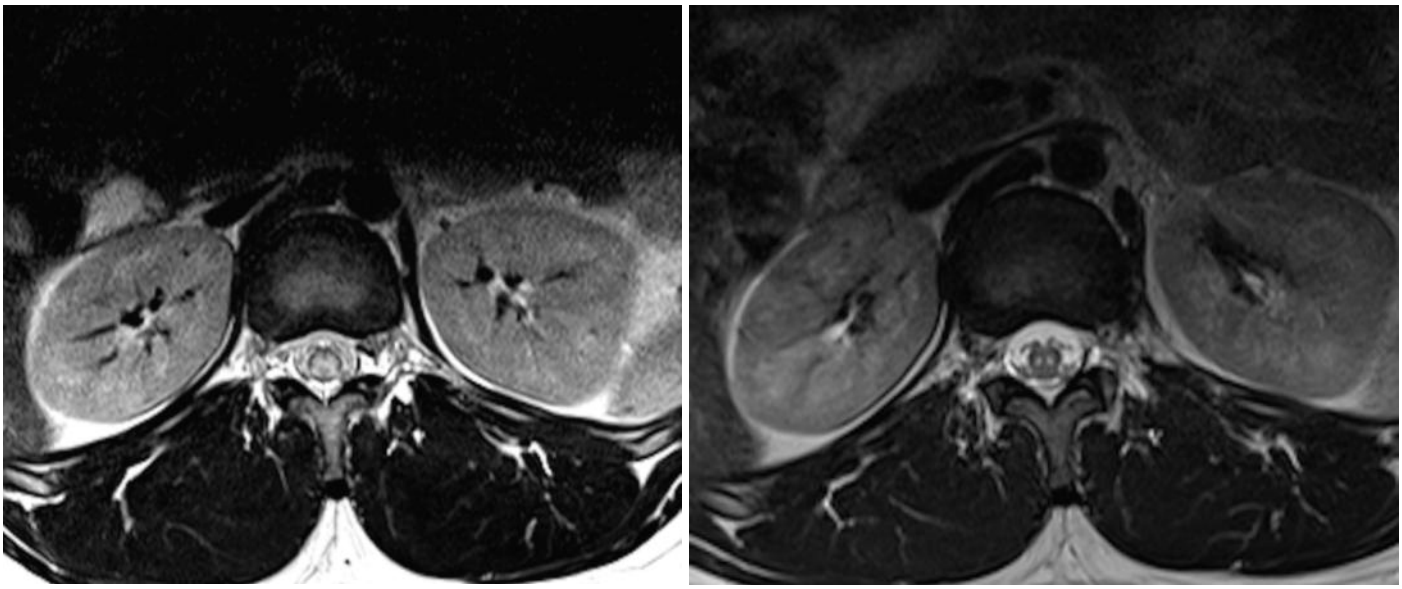

Figure 2. MRI comparison of the distal spinal cord during hospitalization and at 4-month follow-up. Axial T2W image obtained at the time of hospitalisation (A) reveals significant cord expansion and abnormal hyperintensity within the cord. Axial T2W image of the distal cord four months later reveals significant regression of the signal abnormality and resolution of the previously noted cord edema (B).

menon involving dynamic compression, vasospasm or thrombotic infarction of the artery of Adamkiewicz, which occurs as the result of hyperextension of the spinal cord while individuals are lying prone on a surfboard [1-4]. From the aorta, branches of the posterior intercostal arteries arise which provide vascular supply to the spinal cord as single anterior and dual posterior spinal arteries. The distinctly dominant caliber segment of the anterior spinal artery is termed the artery of Adamkiewicz. An anatomical watershed zone susceptible to ischemia is identified in the midthoracic region of the cord from T3 to T8 levels due to poor intercostal artery vascularization [5]. Transient spinal cord ischemia of the watershed zone affects the activity involving the abdomen and legs, especially in surfers, caused by steal from the spinal cord territory for which blood flow had been reduced [6]. Inferior vena cava obstruction and fibrocartilaginous embolism have also been proposed in the pathogenesis. It is postulated that the inferior vena cava is compressed by the liver while lying on a surfboard and prolonged valsalva maneuver during paddling may lead to increased retrograde pressure in the epidural venous plexus leading to infarction [1, 5]. Fibrocartilaginous embolism into a spinal artery can result from increased intradiscal pressure from axial loading of the spine produced by hyperextension.

MRI is a non-invasive diagnostic imaging modality of choice for the evaluation of Surfer's myelopathy and typically demonstrates abnormal increased T2 signal and swelling of the central spinal cord. There is usually absent or trace enhancement following gadolinium contrast administration [3, 7-8]. The region of involvement can be as short as from the conus to T10 or extend to the mid thoracic region [3].

Early MRI (within 3 hours) may be normal because the cytotoxic edema producing the abnormal T2 signal takes some time to develop. In addition, good collateral blood supply may be present in the affected region [7]. Early detection of spinal cord ischemia and/or infarction may be improved by using diffusion weighted imaging (DWI), which can reveal spinal cord ischemia in the acute stage when T2-weighted can be normal

[7-8]. However, DWI in spinal cord lesions has been technically limited due to susceptibility artifacts, movement and the small size of the spinal cord [7]. Angiography may be performed to evaluate vascular occlusion or to exclude an underlying arteriovenous malformation, however this is only recommended if there is no improvement in the neurologic symptoms.

The imaging and clinical presentation of spinal cord ischemia and infarction can be similar to other spinal cord diseases, particularly transverse myelitis. In idiopathic transverse myelitis, the symptoms are usually preceded by a viral illness or vaccination, [3]. Our patient was previously well without a history of a recent viral disease or vaccination and had been surfing within 24 hours of symptoms onset. Multiple sclerosis, (MS) is another differential diagnosis consideration but typically involves the dorsolateral regions of the cord and can have brain involvement [3, 5]. The abnormal T2 signals noted in our patient are located in the centromedullary portion of the spinal cord. Furthermore, our patient did not have the clinical manifestations of MS and his symptoms responded to steroid therapy without progression or sequelae.

Conclusion

In summary, we present a case of an adolescent male with clinical and MRI manifestations of Surfer's myelopathy with increased T2 signal in the centromedullary region of the spinal cord which is a pattern of abnormality similar to that described in adult cases. With the growing popularity of surfing as a sport, it is important for radiologists to be familiar with the clinical and imaging manifestations of this condition.

References

1. Karabegovic A, Strachan-Jackman S, Carr D (2011) Surfer's Myelopathy: Case Report and Review. Canadian Journal of Emergency Medicine 13(5): 357-360
2. Thompson TP, Pearce J, Chang G, Madamba J (2004) Surfers' Myelopathy. Spine 29(16): E353-356
3. Nakamoto BK, Siu AM, Hashiba KA, et al (2013). Surfer's Myelopathy A Radiologic Study of 23 Cases. AJNR Am J Neuroradiol 34(12):2393-8
4. Kelly M, Wright KM (2010) A Case of Surfer's Myelopathy. American Journal of Clinical Medicine 7 (2): 74-75
5. Aviles-Hernandez I, Garcia-Zozaya I, DeVillasante JM (2007) Non-traumatic Myelopathy Associated with Surfing. J Spinal Cord Med 30: 288-293
6. Chiesa R, Melissano G, Bertoglio L, et al (2008) The Risk of Spinal Cord Ischemia during Thoracic Endografting. Acta Chir Belg 108: 492-502
7. Alblas CL, Bouvy WH, Nijeholt GJL and Boiten J (2012) Acute Spinal Ischemia: Evolution of MRI Findings. Journal of Clnical Neurology 8: 218-223
8. Chang CW, Donovan DJ, Liem LK, et al (2012) Surfers' myelopathy: a case series of 19 novice surfers with non traumatic myelopathy. Neurology 27;79(22):2171-6. doi:10.1212/WNL.0b013e31827595cd. Epub 2012 Nov 14

Corresponding Author:
Mariaem M. Andres, MD
email: mariaem139@yahoo.com

Runs in the family: A Case of Familial Hypertrophic Cardiomyopathy with Atypical Location.

Jeremiah A. Sarmiento, MD-MBA and Jasmine Marie E. Arzadon, MD, FPCR
The Medical City, Ortigas, Pasig City, Philippines

Abstract

Hypertrophic cardiomyopathy is one of the most commonly inherited cardiovascular diseases in the world. One of its pathogenesis is linked to familial inheritance, hence the name, familial hypertrophic cardiomyopathy. This research evaluated two patients who were diagnosed with hypertrophic cardiomyopathy based on clinical findings, echocardiography and transthoracic echocardiogram. These patients then underwent cardiac MRI revealing asymmetric hypertrophy for the 1st case and an atypical location hypertrophic cardiomyopathy for the 2nd case. Taken together, for evaluation of patients with familial hypertrophic cardiomyopathy, the use of cardiac MRI is commendable in identifying hypertrophy of myocardial segments that were not detected in other diagnostic procedures. Identifying the involved segments in hypertrophic cardiomyopathy is vital for the prognosis of patients as well as the proper intervention they need.

Introduction

Hypertrophic cardiomyopathy (HCM) is the most commonly inherited cardiovascular disease with a prevalence of 1:500 in the population. It is a frequent cause of sudden cardiac disease (SCD) in the pediatric population and among young athletes. According to Noureldin et. al., the expression of HCM may occur at any age, however, it is during adolescence where phenotypic expression is the highest. Therefore, clinical screening of first-degree relatives annually is ideal in this age group (12-18 years old) [1].

The condition manifests as abnormal ventricular wall thickening, defined by left ventricular (LV) wall thickness (≥ 15mm at end diastole in one or more myocardial segments). Furthermore, a septal to lateral wall thickness ratio beyond 1.3 is likewise diagnostic. It is important to note that the cause of wall thickening should not be secondary to diseases such as hypertension or aortic valve stenosis [2]. The degree of wall thickening may be symmetric or asymmetric [3]. HCM is transmitted from parent to offspring via an autosomal dominant pattern of inheritance. The genes that are transmitted encode contractile apparatus of the heart muscles, particularly the sarcomeric proteins. The wide array of sarcomeric mutations with varying phenotypes produces a thickened myocardium [4].

Case Report

This is a case of 2 siblings with a family history of hypertrophic cardiomyopathy (familial hypertrophic cardiomyopathy). Their mother died at the age of 30 and an older female sibling at the age of 16, both succumbing to sudden cardiac death secondary to HCM. Both siblings underwent transthoracic echocardiogram (TTE) and cardiac MRI (CMR) which revealed an asymmetric form of HCM for the first sibling and HCM with atypical location (inferior segment involvement) for the second.

Patient 1

Y.E. is a 16-year-old female who presented with episodes of palpitations, difficulty of breathing and chest discomfort. During her consultation, an ECG was done revealing sinus bradycardia (56 beats per minute) and left ventricular hypertrophy with strain pattern. A transthoracic echocardiogram (TTE) was subsequently performed showing thickening of the LV septum and apex with reduction of the left ventricular cavity. There is diastolic dysfunction of the left ventricle, however, the LV systolic function is preserved with no evident ventricular outflow obstruction. A CMR was then requested for further evaluation.

Cardiac MRI Findings

The cardiac chambers exhibit normal systemic and pulmonary venous return. Likewise, the cardiac valves show normal features. The size of the left ventricular cavity is less compared to right but still exhibits normal systolic function. Asymmetric hypertrophy of the following segments were noted (Figure 1):

1. Basal to apical anterior
2. Basal and mid anterior septum
3. Basal and mid inferior septum
4. Mid and apical inferior

The most thickened segment is identified on the mid inferior septum measuring 3.8 cm. The right ventricle is normal in size and has normal systolic function. There are no segmental wall motion abnormalities identified in the ventricles. However, left atrial dilatation is appreciated.

Myocardial tissue characterization showed no evidence of fatty infiltration or edema. On delayed enhancement studies, there is patchy intramyocardial enhancement involving the basal to apical anterior, basal and mid inferior septum and midapical inferior segments as well as the anterior septum at the level of the right ventricular insertion point, which indicates myocardial fibrosis along these segments (Figure 2).

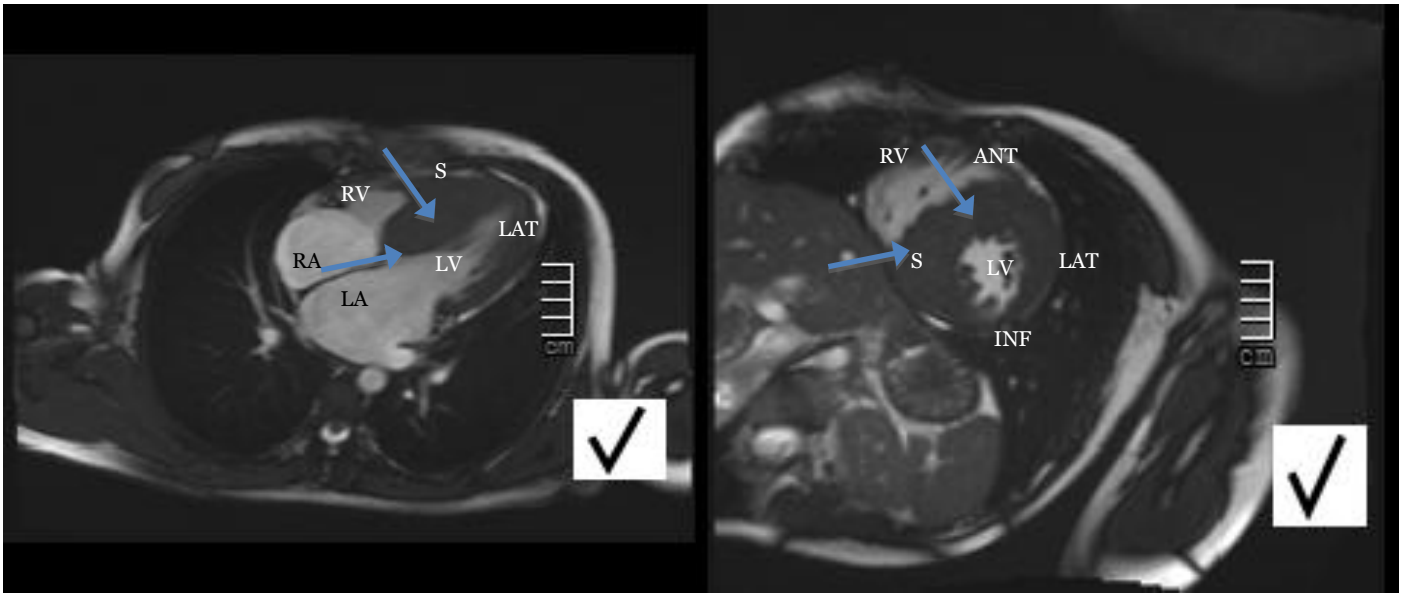

Figure 1. Spin echo images showing horizontal (left) and short (right) axis views demonstrating asymmetric hypertrophy of the basal to apical anterior, basal and mid anterior septum, basal and mid inferior septum as well as the mid and apical inferior segments. Legend: RA = Right atrium, RV = Right ventricle, LA = Left atrium, LV = Left ventricle, S = Septum, LAT = Lateral wall, ANT = Anterior wall, INF = Inferior wall

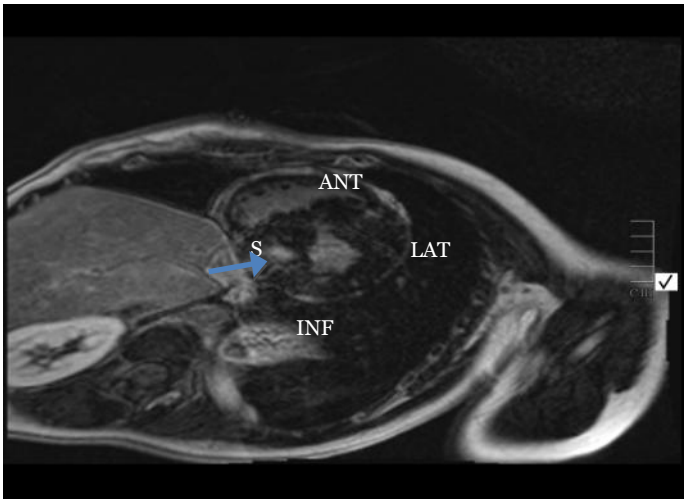

Figure 2. Delayed enhanced, short-axis image showing fibrosis of the basal to apical anterior, basal and mid inferior septum and midapical inferior segments as well as the anterior septum (represented by late gadolinium enhancement depicted as areas of lesser hypointensity).

Patient 2

Z.E. is a 13-year-old male who was also evaluated for easy fatigability. During his consultation, an ECG was also performed showing normal sinus rhythm (72 beats per minute) as well as left ventricular hypertrophy with strain pattern. TTE results revealed septal wall hypertrophy with maximal thickness in the mid-septum. There is evidence of left ventricular outflow obstruction as a result of systolic anterior motion (SAM) of the mitral valve. The biventricular function is maintained with preservation of LV diastolic and systolic function. CMR was requested at the time for better characterization

Cardiac MRI Findings

All the cardiac chambers demonstrate normal sizes with no segmental wall motion abnormalities. The left ventricular cavity has normal size and systolic function with asymmetric hypertrophy of the inferior segments as follows (Figure 3):

1. Basal to apical inferior
2. Basal to mid inferoseptal
3. Apical septum

The mid inferoseptal segment shows the most area of thickening as it measures 3.2 cm in maximal thickness. There is no evidence of systolic anterior motion of the mitral valve, a contradictory finding from the previous TTE. The right ventricle is normal in size with normal systolic function.

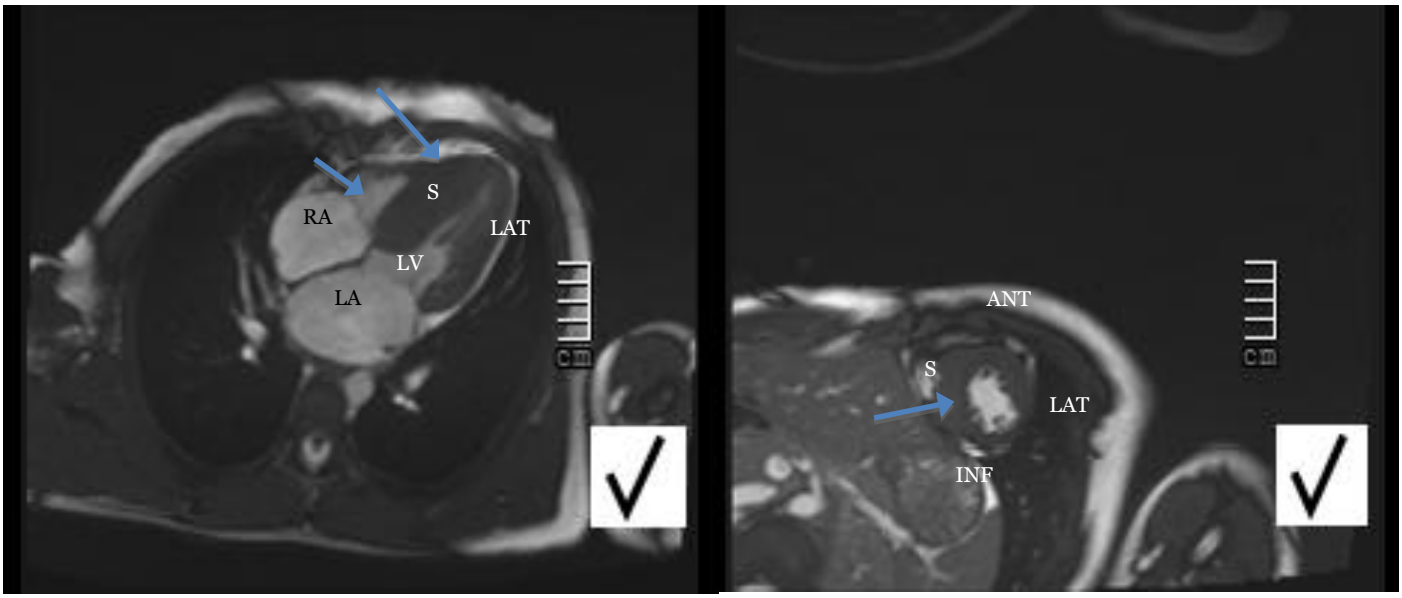

Figure 3. Spin echo images showing horizontal (left) and short (right) axis views demonstrating asymmetric hypertrophy of the basal to apical inferior, basal to mid inferoseptal as well as the apical segments.

Myocardial tissue characterization showed no evidence of fatty infiltration or edema. On delayed enhancement studies, there is patchy intramyocardial enhancement involving the basal to apical inferior and basal to mid inferoseptal segments as well as the apical septum. These findings pertain to intramyocardial fibrosis or scarring (Figure 4).

Discussion

HCM is defined as unexplained left ventricular hypertrophy (LVH) and exhibits a myriad pattern of wall thickening. The magnitude of LV wall thickness is significant in prognosticating the clinical outcome of the disease showing a direct relationship to the risk of cardiac death [5]. HCM is a complex disease entity presenting in a variety of phenotypes, which eventually manifests with complex cardiac symptoms. The penetrance of LVH is age-dependent. LVH often develops during adolescence or young adulthood. However, LVH can develop late in life, in infancy, and in early adulthood [6].

The presentation of the disease ranges from being asymptomatic and symptoms that predisposes these patients from arrhythmias and SCD [7].

Noureldin et. Al [1] described at least 5 variants of HCM based on their appearances in CMR including asymmetric HCM with sigmoid septal contour (septal HCM), asymmetric HCM with reversed septal contour, HCM with midventricular obstruction, apical HCM and symmetric HCM. The most common form of the disease, comprising two-thirds of the population with HCM, is the asymmetric HCM with sigmoid septal contour type. It is characterized by hypertrophy of the anteroseptal myocardium resulting to a sigmoidal contour of the septum. Structural abnormalities such as SAM and mitral leaflet-septal contact are common in this form that may lead to left ventricular outflow tract obstruction (LVOT).

There is heterogeneity in the localization and number of involved myocardial segments in HCM. The most common segments include the interventricular septum and anterolateral free wall while the involvement of the inferoseptum and the inferior wall are deemed rare and atypical. The case in this study (Patient 2) presented with hypertrophy of the inferior wall segments, hence he was classified as HCM with atypical location. In a study done by Guler et. Al [8], the overall outcome of familial hypertrophic cardiomyopathy are not solely based on the involved segments. Rather, correlation with other parameters such as symptomatology, ECG and TTE results as well as CMR findings is relevant for prognostication.

Prior to the use of non-invasive imaging modalities such as echocardiogram (echo) and cardiac MRI (CMR) the diagnosis of HCM was solely based on autopsy findings [1]. However, with the advent of non-invasive techniques, in vivo diagnosis of HCM became attainable [2]. HCM is now most often diagnosed through non-invasive cardiac imaging such as echocardiography and cardiac magnetic resonance imaging (cardiac MRI). Others may included histopathology, family history and genetic testing.

According to Rickers C, et al [5], although 2D Echocardiography is the standard imaging modality for clinical identification of the LV hypertrophy, a small number of patients affected by HCM are not diagnosed. Echocardiography has certain technical limitations such as quantitative delineation of the LV wall thickness which is dependent on adequate acoustic windows. Another is that echocardiographic trans-

ducer is often at a fixed point on the anterior chest wall that obliquity is difficult to be avoided. CMR has the capability of acquiring tomographic images of the hypertrophied LV chamber, with tissue contrast and border definition that are often superior to that of echocardiography. It has the potential to detect segmental wall thickening in any area of the LV wall, even if these regions are limited in size, and therefore can provide critical supplemental morphological information, beyond that obtained from conventional and clinically adequate echocardiographic studies.

As with our two case studies, in conjunction with the echocardiographic results, CMR was able to better delineate the extent of the areas of hypertrophy and identify areas of fibrosis/ischemia.

The current use of echocardiography and CMR are not only limited to the diagnosis of HCM but also provide phenotype characterization, cardiac function assessment, disease severity classification/risk stratification, tool for screening and a guide for therapy [9].

For the patients involved in this case, they are currently managed with activity restriction and medical management with beta-blockers. Given that there is no significant left ventricular outflow obstruction upon confirmation from TTE and CMR findings, surgical myomectomy is not indicated [10]. Constant surveillance and follow-up is needed to monitor disease progression.

Conclusion

Early screening and detection of HCM is crucial particularly to patients with a known family history of the disease and presenting with cardiac symptoms. Screening with echocardiography and confirmation of findings via CMR are useful tools in providing appropriate intervention for affected patients in order to delay disease progression and prevent SCD.

References

1. Noureldin RA, Liu S, Nacif MS, et. al. The diagnosis of hypertrophic cardiomyopathy by cardiovascular magnetic resonance. Journal of Cardiovascular Magnetic Resonance, 2012; 14:17. http://www.jcmr-online.com/content/14/1/17.

2. Morita Y, Kato T, Okano M, et. al. A rare case of hypertrophic cardiomyopathy with subendocardial late gadolinium enhancement in an apical aneurysm with thrombus. Case Reports in Radiology. 2014; Vol 2014, Article 780840: 5 pages.

3. Dillman JR, Mueller GC, Attili AK, et. al. Case 153: Atypical tumefactive hypertrophic cardiomyopathy. Radiology 2010; Vol 254, Issue 1: 310-13.

4. Watkins H, Ashrafian H, Redwood C. Inherited cardiomyopathies. The New England Journal of Medicine. 2011; 364: 1643-1656.

5. Rickers C, Wilke NM, Jerossch-Herold M, et al. Utility of Cardiac Magnetic resonance imaging in the diagnosis of Hypertrophic cardiomyopathy. Circulation, 2005; 112 (6): 855-61.

6. Cirino AL, Ho C. Hypertrophic Cardiomyopathy Overview. 2008 Aug 5 [Updated 2014 Jan 16]. In: Pagon RA, Adam MP, Ardinger HH, et al., editors. GeneReviews® [Internet]. Seattle (WA): University of Washington, Seattle; 1993-2016. Available from: http://www.ncbi.nlm.nih.gov/books/NBK1768

7. Pantazis A, Vischer AS, Perez-Tome MC, et. al. Diagnosis and management of hypertrophic cardiomyopathy. Echo Research and Practice. 2015; Volume 2: Number 1: R45-53.

8. Guler A, Tigen KM, Aung SM, et. al. Familial hypertrophic cardiomyopathy with atypical location: Diagnosis by means of echocardiography and cardiovascular magnetic resonance. Texas Heart Institute Journal. 2012; 39(1): 138-139.

9. Chun EJ, Choi SI, Jin KN, et. al. Hypertrophic cardiomyopathy: Assessment with MR Imaging and Multidetector CT Radiographics. 2010; Vol 30, Issue 5: 1309-1328.

10. Yetman AT, McCrindle BW. Management of pediatric hypertrophic cardiomyopathy. Current Opinion in Cardiology. 2005; 20: 80-83.